Inorganic Chemistry
Cite This: Inorg. Chem. XXXX, XXX, XXX−XXX
Article
pubs.acs.org/IC

Binucleating Hydrazonic Ligands and Their μ-Hydroxodicopper(II) Complexes as Promising Structural Motifs for Enhanced Antitumor Activity

Jesica Paola Rada,[†] Beatriz S. M. Bastos,[†] Luciano Anselmino,[‡] Chris H. J. Franco,[§] Mauricio Lanznaster,[∥] Renata Diniz,[⊥] Claudio O. Fernández,[‡] Mauricio Menacho-Márquez,[‡] Ana Maria Percebom,[†] and Nicolás A. Rey*[,†]

[†]Pontifical Catholic University of Rio de Janeiro, Rio de Janeiro, 22451-900, Brazil

[‡]Max Planck Laboratory for Structural Biology, Chemistry and Molecular Biophysics of Rosario (MPLbioR, UNR-MPIbpC) and Instituto de Investigaciones para el Descubrimiento de Fármacos de Rosario (IIDEFAR, UNR-CONICET), Universidad Nacional de Rosario, S2002LRK Rosario, Argentina

[§]Federal University of Juiz de Fora, Juiz de Fora, 36036-900, Brazil

[∥]Fluminense Federal University, Niterói, 24020-150, Brazil

[⊥]Federal University of Minas Gerais, Belo Horizonte, 31270-901, Brazil

Supporting Information

ABSTRACT: Very few inorganic antineoplastic drugs have entered the clinic in the last decades, mainly because of toxicity issues. Because copper is an essential trace element of ubiquitous occurrence, decreased side effects could be expected in comparison with the widely used platinum anticancer compounds. In the present work, two novel hydrazonic binucleating ligands and their μ-hydroxo dicopper(II) complexes were prepared and fully characterized. They differ by the nature of the aromatic group present in their aroylhydrazone moieties: while H_3L1 and its complex, **1**, possess a thiophene ring, H_3L2 and **2** contain the more polar furan heterocycle. X-ray diffraction indicates that both coordination compounds are very similar in structural terms and generate dimeric arrangements in the solid state. Positive-ion electrospray ionization mass spectrometry analyses confirmed that the main species present in a 10% dimethyl sulfoxide (DMSO)/water solution should be $[Cu_2(HL)(OH)]^+$ and the DMSO-substituted derivative $[Cu_2(L)(DMSO)]^+$. Scattering techniques [dynamic light scattering (DLS) and small-angle X-ray scattering] suggest that the complexes and their free ligands interact with bovine serum albumin (BSA) in a reversible manner. The binding constants to BSA were determined for the complexes through fluorescence spectroscopy. Moreover, to gain insight into the mechanism of action of the compounds, calf thymus DNA binding studies by UV−visible and DLS measurements using plasmid pBR322 DNA were also performed. For the complexes, DLS data seem to point to the occurrence of DNA cleavage to Form III (linear). Both ligands and their dicopper(II) complexes display potent antiproliferative activity in a panel of four cancer cell lines, occasionally even in the submicromolar range, with the complexes being more potent than the free ligands. Our data on cellular models correlate quite well with the DNA interaction experiments. The results presented herein show that aroylhydrazone-derived binucleating ligands, as well as their dinuclear μ-hydroxodicopper(II) complexes, may represent a promising structural starting point for the development of a new generation of highly active potential antitumor agents.

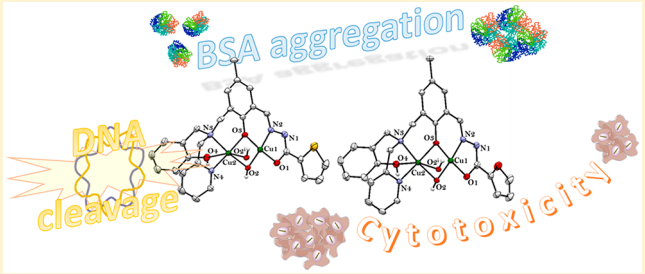

INTRODUCTION

Since the fortuitous discovery of the antitumor activity of cisplatin by Rosenberg et al.[1] in the second half of the 1960s, the search for new metal-based anticancer agents has increased dramatically. In spite of this, very few new inorganic antineoplastic drugs have entered the clinic in the last decades, mainly because of toxicity issues. In this context and because copper is an essential trace element of ubiquitous occurrence, decreased side effects could be expected in comparison with the widely used platinum anticancer compounds cisplatin, carboplatin, and oxaliplatin.[2] Moreover, because of the fundamental differences between the chemistry of copper complexes and those of platinum, one can also expect diverse mechanisms of action. In a very recent Perspective published by Wehbe and co-workers,[3] the potentiality of copper complexes as a novel class of therapeutics for an extensive range of diseases, including cancer, is discussed. The paper

Received: April 24, 2019

DOI: 10.1021/acs.inorgchem.9b01195
Inorg. Chem. XXXX, XXX, XXX−XXX

comments on Casiopeinas,[4,5] a series of mononuclear mixed-chelate copper-based antineoplastic compounds that have entered phase I clinical trials in Mexico. In such a highly active field of research, a large variety of ligands have been used to synthesize copper complexes with potential antiproliferative action. Santini and co-workers[6] published a comprehensive review about coordination compounds of this metal reported between 2008 and 2012 as having antitumor activity. Even more recently, cytotoxic copper complexes comprising a diversity of ligands have been described, among them hydrazides and N,N-heterocycles,[7] derivatives of coumarin,[8] aroylhydrazones,[9] thiosemicarbazones,[10] β-diketones and N-heterocycles,[11] phenanthroline,[12] tripodal pyrazolylamines,[13] nalidixic acid,[14] benzimidazoles,[15,16] fluoroquinolones,[17] and a 1,2,4-triazole-derived Schiff base.[18] In some cases, their ability to induce apoptotic cell death was demonstrated.[7,14,16,17] The capacity to interact with DNA and the DNA-cleaving properties of copper compounds have also been confirmed.[14,15,19−23] For example, Patil et al.[22] synthesized a series of cobalt, nickel, and copper complexes using the same organic ligands and showed that the copper(II) derivatives possess a better cleavage activity than the corresponding cobalt and nickel compounds.

During the past decade, the use of dicopper(II) compounds has constituted an interesting tendency in this area because bimetallic copper cores are abundant in nature. A typical example is that of catechol oxidases (COs), a group of ubiquitous type 3 dicopper enzymes. The crystal structure of the sweet-potato CO was already described and possesses, in its resting $Cu^{II}Cu^{II}$ state, two cupric ions bridged by an exogenous hydroxo ligand.[24] This result triggered scientific interest in the synthesis of biomimetic models for the active site of COs.[25,26] Some years ago, we demonstrated that, in addition to the predictable catecholase-like activity, these CO-inspired complexes display phosphate diester hydrolysis activity, which makes them promiscuous catalysts.[27] The catalytic mechanism of hydrolysis probably involves terminal coordination of the phosphate diester to one of the cupric ions and subsequent intramolecular nucleophilic attack by the bridging hydroxide.[28,29] The phosphatase-like activity was proven in plasmid DNA (as well the nuclease activity), suggesting that this class of compounds could also perform properly as potential antineoplastic agents. This was, in fact, confirmed toward the GLC4 (small-cell lung carcinoma) and K562 (myelogenous leukemia) cell lines.[30] In the past few years, several other dicopper(II) complexes have been synthesized and studied regarding their anticancer properties. Some authors demonstrated the DNA binding[31−43] and/or DNA cleavage[33,36,42,44,45] abilities of these compounds. Very recently, Cao et al. proved that alteration of the chelating arms on the ligands allows for regulation of the reactivity of their dinuclear copper(II) complexes toward DNA.[46] The in vitro antiproliferative activity of novel dicopper(II) compounds has also been tested. As an example, the complexes synthesized by Godlewska and co-workers showed a moderate antineoplastic activity in U937 cells.[47] However, in most cases, those compounds presented a better antiproliferative profile than cisplatin itself. In this sense, the authors reported new complexes with IC_{50} values in the micromolar range for HepG2 cancer cells.[35−39] Additionally, remarkable activities have been described in the HeLa and A549,[35] SMMC-7721,[39] and MGC-803 and BEL-7404[43] cell lines. In other studies, the compounds have shown even lower IC_{50} values, in the nanomolar range, when tested in HeLa and Caco-2,[41] as well as in U937[42] and MCF7,[48] cells. Some of these works have reported the induction of apoptosis as a putative mechanism of action.[43,45]

However, regardless of the large number of promising reports on the antiproliferative effects of copper(II) complexes, their poor aqueous solubility,[3] as well as an in vivo decreased activity related to their extensive and nonselective binding to biomolecules[49] (a process known as "speciation"), creates an additional barrier for the compounds' translation into clinical trials. In order to overcome these difficulties, recent studies have shown the benefit of encapsulating copper(II) complexes in nanoliposomes, with encouraging results.[3,49]

On the other hand, aroylhydrazones constitute a diverse family of bidentate nitrogen-and oxygen-donor atoms with a vast spectrum of biological activities.[50] Our hypothesis is that modifying previously known compartmental ligands, such as 3-[(2-hydroxybenzyl)(2-pyridylmethyl)amine]-2-hydroxy-5-methylbenzaldehyde (HBPAMFF),[51,52] through the addition of an aroylhydrazone moiety represents a simple way to develop a set of versatile unsymmetrical binucleating ligands. These ligands allow for the synthesis of interesting novel dicopper(II) compounds displaying different geometries and even distinct coordination numbers at each cupric center. In fact, in a current publication by the research group of Belle,[53] two new unsymmetrical ligands derived from bis(2-pyridylmethyl)aminomethyl-2-hydroxy-5-methyl benzaldehyde and 4-methyl or 4,4-dimethyl 3-thiosemicarbazide, as well as their dinuclear and tetranuclear phenoxo-bridged copper(II) complexes, were described and extensively studied by structural, spectroscopic, electrochemical, and electrospray ionization mass spectrometry (ESI-MS) methods.

In this stimulating scenario and motivated by the search of novel structural motifs for the development of potential antiproliferative agents, the present work describes the first two hydroxo-bridged dicopper(II) complexes containing unsymmetrical hydrazonic binucleating ligands and evaluates them as candidates for prospective antitumor drugs.

EXPERIMENTAL SECTION

Chemicals. Acetone (DMK), acetonitrile (ACN), diethyl ether (Et_2O), dimethyl sulfoxide (DMSO), dichloromethane (DCM), ethanol (EtOH), methanol (MeOH), isopropyl alcohol (iPrOH), triethylamine (Et_3N), sodium tetrahydroborate ($NaBH_4$), hydrochloric acid (HCl), chloroform, anhydrous sodium sulfate, sodium chloride (NaCl), and potassium hydroxide (KOH) were obtained from Vetec (Sigma-Aldrich); copper(II) perchlorate hexahydrate [$Cu(ClO_4)_2{\cdot}6H_2O$] and sodium bicarbonate ($NaHCO_3$) were purchased from Sigma-Aldrich; tris(hydroxymethyl)aminomethane (Tris) was acquired from BIO-RAD; furan-2-carbohydrazide (FCH) and thiophene-2-carbohydrazide (TCH) were purchased from Acros Organics and Sigma-Aldrich; bovine serum albumin (BSA) was purchased from Fluka. Plasmid DNA pBR322 was from Thermo Fisher and calf thymus DNA (ctDNA) sodium salt from Sigma-Aldrich. All of these chemicals were used without any type of treatment or further purification.

Syntheses of Ligands and Their Dicopper(II) Complexes. *Precursors.* The synthesis of the pendant arm (2-hydroxybenzyl)(2-pyridylmethyl)amine (HBPA) from 2-(aminomethyl)pyridine and 2-hydroxybenzaldehyde has been previously reported.[54,55] The conditions of the reaction were slightly modified or optimized in the present study: 2-(aminomethyl)pyridine (7.9 g, 73 mmol) and 2-hydroxybenzaldehyde (7.7 mL, 73 mmol) were stirred in 50 mL of MeOH for 1 h, with the subsequent gentle, portionwise addition of solid $NaBH_4$ (2.8 g, 73 mmol) at 0 °C. The mixture was stirred

DOI: 10.1021/acs.inorgchem.9b01195
Inorg. Chem. XXXX, XXX, XXX−XXX

Scheme 1. Synthesis of the Chemical Precursors HBPA and HBPAMFF, the Binucleating Ligands H_3L1 and H_3L2, and Their Respective μ-Hydroxodicopper(II) Complexes 1 and 2

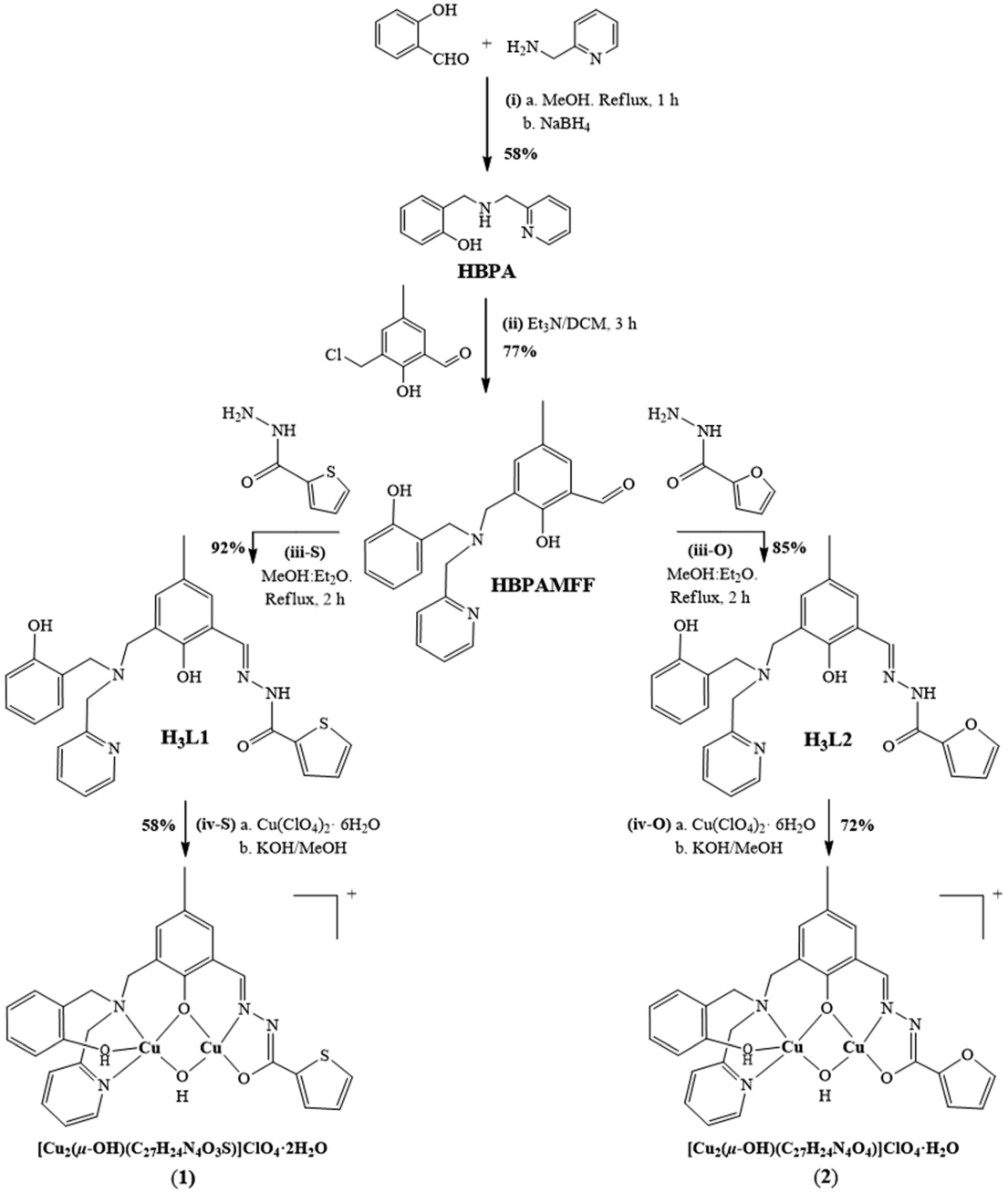

overnight, and then the pH was adjusted to 5−6 with a 4 mol L^{-1} HCl aqueous solution. The solvent was removed under reduced pressure on a rotary evaporator at 45 °C and the product redissolved in 60 mL of chloroform and then washed with 5 × 40 mL portions of a saturated $NaHCO_3$ solution and once with water, waiting 15 min between the separations. The product was extracted with chloroform (3 × 30 mL) and the organic phase dried over anhydrous sodium sulfate. Chloroform was evaporated and the product allowed to stand in Et_2O in a freezer for 3 days. A colorless crystalline solid was separated.

Mp = 63 °C. Yield = 9.0 g (42 mmol, 58%).

Precursor HBPAMFF was synthesized as described previously[51] from HBPA and (2-chloromethyl-4-methyl-6-formyl)phenol (CMFF),[56] according to the following modified conditions: HBPA (2.3 g, 10.4 mmol) and Et_3N (1.5 mL, 10.4 mmol) were both dissolved together in 40 mL of DCM and then slowly added at 0 °C to 40 mL of a CMFF (2.0 g, 10.4 mmol) solution in DCM. The mixture was stirred for 3 h at room temperature and then washed and extracted, as described above for HBPA. The product was allowed to stand in iPrOH at −18 °C (freezer conditions) for 12 h, and a white crystalline solid was separated.

Mp = 103−104 °C. Yield = 2.9 g (8 mmol, 77%).

Ligands. ***H_3L1.*** This ligand was prepared by dropwise adding a methanolic solution (10 mL) of TCH (586.3 mg, 4 mmol) to 30 mL of a slightly heated solution containing the precursor HBPAMFF (1.45 g, 4 mmol) in MeOH/Et_2O (1:1). The mixture was left under reflux for 2 h, and after 30 min of cooling, the product was filtered off and washed with ice-cold Et_2O.

Mp = 187 °C. Yield = 1.8 g (3.7 mmol, 92%). Recrystallization in MeOH afforded light-yellow crystals with hexagonal geometry. Optical photographs of **H_3L1** crystals can be found in Figure S1. The single-crystal size was very small for X-ray diffraction (XRD)

DOI: 10.1021/acs.inorgchem.9b01195
Inorg. Chem. XXXX, XXX, XXX−XXX

analysis. Elem anal. Calcd for $C_{27}H_{26}O_3N_4S$ (486.63 g mol^{-1}): C, 66.6; H, 5.4; N, 11.5; S, 6.6. Found: C, 66.1; H, 5.5; N, 11.8; S, 6.7.

H_3L2. This ligand was prepared from FCH (514.7 mg, 4 mmol) in 5 mL of MeOH and HBPAMFF (1.45 g, 4 mmol) following the same procedure as that used to synthesize **H_3L1**.

Mp = 185 °C. Yield = 1.6 g (3.4 mmol, 85%). Light-yellow crystals with hexagonal geometry were obtained by recrystallization in MeOH (Figure S1). Single crystals were analyzed by XRD, but peaks presented low intensity. Elem anal. Calcd for $C_{27}H_{26}O_4N_4$ (470.57 g mol^{-1}): C, 68.9; H, 5.6; N, 11.9. Found: C, 68.4; H, 5.6; N, 12.3.

Copper Complexes. [Cu_2(μ-OH)($C_{27}H_{24}N_4O_3$S)]ClO_4·$2H_2O$ (1). $Cu(ClO_4)_2$·$6H_2O$ (378.1 mg, 1.0 mmol) was dissolved in 3 mL of MeOH and dropwise added to a solution of the **H_3L1** ligand (243.32 mg, 0.5 mmol) in 35 mL of a MeOH/ACN (6:1) mixture. The reactants were heated for 40 min, and then 1 mL of a methanolic KOH solution (1 M, 1 mmol) was added. Heating and stirring were maintained for another 20 min. After 12 h, the green solid was filtered off and washed with ice-cold MeOH. The dry solid was recrystallized in EtOH, affording dark-green crystals (Figure S2) suitable for XRD analysis.

Yield = 220 mg (0.29 mmol, 58%). Elem anal. Calcd for **1** (764.21 g mol^{-1}): C, 42.4; H, 3.8; N, 7.3; S, 4.2. Found: C, 42.9; H, 3.9; N, 7.5; S, 4.0. ICP-OES. Calcd: Cu, 16.6. Found: Cu, 15.8. TGA: for complex **1**, the weight loss was approximately 5.3% (calcd 4.7%) between 25 and 278 °C, corresponding to the removal of two hydration water molecules. Molar conductivity in ACN: 180 Ω^{-1} cm^2 mol^{-1} (1:1 electrolyte system),[57] consistent with the presence of a single perchlorate as the counterion.

[Cu_2(μ-OH)($C_{27}H_{24}N_4O_4$)]ClO_4·H_2O (2). This complex was prepared according to the same procedure as that used to synthesize **1**. Complex **2** was recrystallized in DCM/DMK/EtOH (1:1:1), obtaining dark-green crystals (Figure S2) suitable for XRD analysis.

Yield = 266 mg (0.36 mmol, 72%). Elem anal. Calcd for **2** (730.12 g mol^{-1}): C, 44.4; H, 3.7; N, 7.7. Found: C, 44.0; H, 3.7; N, 7.4. ICP-OES. Calcd: Cu, 17.4. Found: Cu, 17.3. TGA: in the case of **2**, the weight loss between 25 and 221 °C was in accordance to the elimination of only one hydration water molecule. Molar conductivity in ACN: 144 Ω^{-1} cm^2 mol^{-1} (1:1 electrolyte system),[57] consistent with the presence of a single perchlorate as the counterion.

Caution! *Perchlorate salts of metal complexes containing organic ligands are potentially explosive and should be handled with care. Only small amounts should be prepared.*

The whole synthetic route described in this section is summarized in Scheme 1.

Measurements. *Spectroscopic Studies.* UV−visible spectra over the wavelength range 900−250 nm were recorded in a PerkinElmer Lamba 35 spectrophotometer and an Agilent Cary 100 spectrophotometer, after dissolving the compounds in DMSO or 10% DMSO in water. The binucleating ligands were characterized by 1D and 2D NMR spectroscopy. The spectra were recorded on a Bruker Avance III HD-400 spectrometer and calibrated with reference to the residual peaks for DMSO-d_6: 2.50 (^{1}H) and 39.52 (^{13}C) ppm. *J* coupling constants are given in hertz. Chemical shifts are reported in parts per million. Spectra were processed by using the *TopSpin 3.5* software.

Mid-infrared vibrational spectra were acquired on a PerkinElmer Spectrum 400 Fourier transform infrared (FTIR) spectrophotometer, at room temperature, in KBr pellets, with a resolution of 4 cm^{-1} in the 4000−450 cm^{-1} range. Each measurement corresponds to a total of 16 scans. The spectra were processed by using the PerkinElmer *Spectrum 10.03.09* software. On the other hand, Raman spectra were collected at room temperature by using a micro-Raman confocal Horiba Xplora ONE Jobin Yvon spectrometer with a spectral resolution of 10 cm^{-1} in the 3500−700 cm^{-1} range. The Raman microscope was equipped with a charge-coupled-device (CCD) detector and with an integrated camera and a Kohler illumination for transmission and reflection illumination. The laser beam was focused onto the samples through a microscope objective of 50×. Different lasers were used as the excitation source: 532 nm (for the ligands) and 785 nm (for the complexes). The samples were placed on quartz sample slides. In order to achieve a sufficient signal-to-noise ratio, Raman spectra were collected in a dark room with an exposure time of 2 s and 20 accumulations. An objective lens with 10× magnification was used to acquire the optical photographs of the compounds. The spectra were processed by using the *LabSpec 6* software, provided by the manufacturer.

X-ray Crystallography. Single-crystal data of complexes **1** and **2** were collected using a Rigaku Agilent SuperNova diffractometer with Mo Kα radiation (λ = 0.71073 Å) at room temperature (293−294 K). Data collection, cell refinement, and data reduction were performed using the *CrysAlisPro* software.[58] The structures were solved and refined using the *SHELXS* and *SHELXL* packages.[59] The method described by Larson[60] was used to refine an empirical isotropic extinction parameter, *x*, by applying a multiscan absorption correction.[61] The structures of the compounds were drawn with the *Mercury* program.[62] All atoms were refined with anisotropic parameters, except hydrogen atoms, which were located from Fourier difference maps, set in calculated positions and refined as riding atoms. For both compounds, disordered solvent molecules were observed in the crystal lattice. Because of this fact, the *SQUEEZE*[63] methodology was applied to obtain a better description of the complexes. In this method, the electronic density of the solvent was removed from the crystal data, which allowed for a description of the compound based on an improved model. Solvent-accessible volumes per unit cell equal to 469 and 282 Å^3 were found for **1** and **2**, respectively. These results agree with elemental analyses of the compounds, which indicate 2 mol of crystallization water molecules in complex **1** but only 1 mol in complex **2** because the voids in the former are almost twice the size of those observed in the latter.

CHNS and Copper Content. Elemental analysis was performed to determine the CHNS content in ligands and complexes on a ThermoElectron analyzer (model Flash EA 1112). All of the measurements were carried out in triplicate with 1% as the maximum standard deviation. The copper content in the complexes was estimated using inductively coupled plasma optical emission spectrometry (ICP-OES; PerkinElmer Optima 7300 DV). Samples were treated with nitric acid and diluted in water. Measurements were performed with a dye laser pulsed in the 324.7 nm line.

ESI-MS Analyses. ESI-MS analyses were carried out on a PerkinElmer SQ-300 mass spectrometer. Stock solutions containing the samples were prepared by dissolving 1.0 mg of the compounds in 100 μL of DMSO (MS grade) and diluting the initial solutions by the addition of 900 μL of deionized water. Both **H_3L1** and **H_3L2** ligands precipitated after the dilution step. Thus, 900 μL of MeOH (MS grade) was used in the preparation of the ligands' stock solutions instead of water. Aliquots of 50 μL of the stock solutions of all samples were diluted in 950 μL of MeOH and analyzed by direct infusion. Analyses of the stock solutions of the complexes were also performed after 24 h of aging. Standard configuration parameters for the positive mode were used, with the capillary output voltage (CAPEX) set at 50 V. Isotopic patterns were simulated using the Isotope Distribution Calculator and Mass Spec Plotter tool.[64]

Thermogravimetric Analysis (TGA) and Electrical Conductivity. TGA curves were acquired in a PerkinElmer Pyris 1 thermogravimetric analyzer. TGA scans were performed from 25 to 900 °C at 10 °C min^{-1} under a flowing dry-air atmosphere. Curve optimization and calculations were processed in the *Pyris v 8.0.0.0172* software. The conductivity measurements were performed at room temperature in a 650MA electrical conductivity meter. In order to obtain a final concentration of 1 × 10^{-3} mol L^{-1}, the copper(II) complexes were dissolved in ACN.

BSA Binding Studies. The interaction between BSA and the synthesized compounds was confirmed by UV−visible, while binding constants were determined only for the complexes using fluorescence spectroscopy. For the latter measurements, a PerkinElmer LS 55 spectrofluorimeter with an optical light filter corresponding to 50% of light attenuation was used. The excitation wavelength was fixed at 280 nm, and the emission was recorded in the range from 290 to 500 nm. The excitation and emission slits were 6 nm. All measurements were performed at 25 °C. Samples were prepared with a fixed concentration of BSA (1 μM) and by variation of the concentrations

DOI: 10.1021/acs.inorgchem.9b01195
Inorg. Chem. XXXX, XXX, XXX−XXX

of the complexes from 0 to 8 μM. For that, a BSA solution was prepared in a buffer (10 mM Tris-HCl containing 10 mM NaCl, pH 7.40) and stored at 4 °C. The concentration of BSA was determined using the molar absorptivity of 43824 M^{-1} cm^{-1} at 280 nm. Stock solutions of the complexes (1 mM) were prepared in DMSO. Mixtures of BSA and complex **1** or **2** solutions in the appropriate proportions were analyzed after 3 min of incubation at 25 °C. This time point was chosen on the basis of previous preliminary tests performed on the system, which indicated that the equilibrium condition was fully reached upon such a reaction time. For UV−visible measurements, the samples were prepared with a BSA/compound molar ratio of 1:5, and blanks with the same concentration of compounds were subtracted.

DNA Binding Studies. In order to study the interaction of the synthesized compounds with DNA, the corresponding compound DNA binding constant (K_b) was determined by UV−visible spectroscopy. For that, an Agilent Cary 100 spectrophotometer, in the range 600−250 nm, was used. Samples were placed in a quartz cuvette with a 1 cm path length. The absorbance was measured for samples with fixed concentrations of the synthesized compounds (25 μM, 3 mL) and increasing concentrations (0−50 μM) of DNA. The absorbance corresponding to free DNA was subtracted by adding an equal amount of DNA to the samples and reference solution. The stock solution was prepared by dissolving sodium salt ctDNA (2 mg mL^{-1}) in a buffer solution (50 mM Tris-HCl containing 50 mM NaCl, pH 7.40) and keeping the solution cold overnight. The DNA concentration per nucleotide was determined by diluting 20 times an aliquot of the stock solution and using the molar absorptivity value of 6600 M^{-1} cm^{-1} at 260 nm.[65,66] A ctDNA stock solution was stored at −20 °C until use. All samples were analyzed in a proportion of 10% DMSO and 90% Tris-HCl (50 mM, 50 mM NaCl, pH 7.40) at 25 °C. The 260/280 nm absorbance ratio of a ctDNA-diluted (20×) stock solution was 1.8−1.9, indicating that DNA was sufficiently free of protein. Analyses of the ctDNA solution in pure buffer and in mixtures containing 10% DMSO and 90% buffer presented identical spectra.

Scattering Studies. For dynamic light scattering (DLS) experiments, 2 mL of each sample was transferred to dispensable cells, which were incubated for 5 min (BSA samples) or 15 min (DNA samples) at 25.0 ± 0.1 °C inside the instrument, to achieve thermal stabilization. BSA samples were filtered through a poly(tetrafluoroethylene) syringe filter (0.45 μm pore size and 0.25 μm diameter, LCR). As a control, some nonfiltered samples were also tested in order to verify the possibility of the formation of particles with higher hydrodynamic radii. Measurements were carried out using a compact Horiba Scientific SZ-100 nanoparticle analyzer. The instrument was equipped with a semiconductor excitation solid laser (532 nm, 10 mW) light source and photomultiplier-tube detector. The scattering angle (θ) was set at 90°, and each sample was measured 20 times for 120 s at 25.0 ± 0.1 °C. The *SZ-100 Horiba for Windows* software was used to record and fit the correlation functions, obtaining the size distributions and mean hydrodynamic diameters through the *CONTIN* algorithm. The samples were prepared from a stock solution of BSA (essentially fatty acid free), with a concentration of 5 × 10^{-5} M, 100 mM NaCl, and 50 mM Tris buffer, pH 7.40. The BSA concentration in the stock solution was determined by its absorbance at 280 nm (ε = 43824 M^{-1} cm^{-1}). Stock solutions of the dicopper(II) complexes **1** and **2** were prepared in DMSO. Different aliquots of the complexes were added to 2800 μL of a BSA stock solution in order to obtain samples with BSA/complex molar ratios of 1:1, 1:7, 1:14, 1:21, and 1:28. Moreover, an additional volume of DMSO was used to obtain complex/BSA solutions with 10% DMSO. For the sake of comparison, samples containing only BSA in 10% DMSO or only the complexes (in the absence of BSA) in Tris-HCl/NaCl buffer were also analyzed. Ligands/BSA and starting salt/BSA measurements were carried out in a unique BSA/compound molar ratio of 1:28, in order to compare their effect with that caused by the copper complexes on the protein. To evaluate the stability of the copper(II) complex/BSA systems over time, measurements were taken every 3 h for at least 24 h. On the other hand, the DNA stock solution (25 μg mL^{-1}) was prepared in 10 mM Tris-HCl, at pH 7.40. Samples containing DNA with different compounds were set to contain 10% DMSO. For that, the DNA concentration was fixed (2.5 μg mL^{-1}) and the concentrations of the complexes were varied from 0 to 50 μM. The influence of the ligands and $Cu(ClO_4)_2{\cdot}6H_2O$ (50 μM) was also analyzed. Blanks of DNA (in 10% DMSO) and of the tested compounds in the absence of DNA were measured.

For small-angle X-ray scattering (SAXS) measurements, BSA samples were analyzed in the same conditions as those previously described for the DLS technique, excluding sample filtration. All SAXS measurements were performed on the beamline at the Brazilian Synchrotron Light Laboratory (LNLS, Campinas, Brazil). The temperature was set at 25.0 ± 0.5 °C and controlled using a water bath. The sample holder was a mica window cell, and the data frames were collected during exposure intervals of 120 s. The beam wavelength was 1.548 Å. SAXS data were acquired using a 2D X-ray detector (CCD-MAR165; MarResearch USA), and the sample-to-detector distance was 902 mm, covering a scattering vector range of 5 < q < 0.1 nm^{-1}. Experimental curves are represented as the X-ray scattered intensity, $I(q)$, as a function of the scattering vector, q. SAXS experimental data were fitted to the Generalized Gaussian Coil model[67,68] using the *Sasfit* program[69] to calculate the gyration radius, R_g, of BSA in the absence and presence of different concentrations of the complexes and a single concentration of the ligands and $Cu(ClO_4)_2{\cdot}6H_2O$.

Cytotoxicity Assays. *Cell Culture.* In the present study, we used a panel of cell lines to evaluate the antitumoral potential of the described compounds. This panel includes two human colorectal cancer cell lines (HCT116 and HT29), a human triple-negative breast cancer cell line (MDA-MB-231), and a melanoma cell line derived from mice (B16F10). As a nontumoral control, we used Madin-Darby canine kidney cells. All cells were incubated at 37 °C with 5% CO_2 and cultured in a Dulbecco's modified Eagle's medium (DMEM) supplemented with 10% fetal calf serum, penicillin (10 μg mL^{-1}), and streptomycin (100 μg mL^{-1}).

Proliferation. For in vitro studies of cell proliferation inhibition by the different compounds on cells, 5 × 10^3 cells $well^{-1}$ were plated on 96-well culture plates. After attachment, different concentrations of drugs were added and cells were allowed to grow for 36 h. The number of living cells was estimated by the tetrazolium salt reduction method (MTT, Sigma-Aldrich) as described before.[70] Proliferation was expressed as the percentage of control untreated samples. The concentrations of drugs decreasing the cell proliferation by 50% (IC_{50}) were estimated from the absorbance curves as a function of the concentration of the analyzed compound by means of the *GraphPad Prism 7* program. The final concentration of DMSO in the culture media was never higher than 1%, and we have carefully checked that the solvent has no effect on the cell growth at such a low level.

RESULTS AND DISCUSSION

Syntheses. Both ligands, as well as their respective dicopper(II) complexes, were obtained in good yield and in crystalline form. Because of the tetrahedral amine nitrogen atom displaying three different substituents, all of the ligands and complexes were isolated as a pair of optical isomers.

Characterization of the Ligands and Complexes. *Solution NMR of the Ligands.* Ligands were fully characterized using multinuclear NMR. The experimental data set includes, along with 1D ^1H and ^{13}C spectra, COSY, HSQC, and HBMC contour maps. Some representative NMR plots can be found in Figures S3−S8. It is well-known that aroylhydrazone derivatives can present geometric isomerism with respect to the azomethine group as well as amide-related tautomerization processes.[71−73] In both ligands, the *E* isomer is virtually the only one existing. However, duplicated sets of signals in the ^1H and ^{13}C NMR spectra of H_3**L1** indicate the presence, in a DMSO-d_6 solution, of both iminol and amido

DOI: 10.1021/acs.inorgchem.9b01195
Inorg. Chem. XXXX, XXX, XXX−XXX

Scheme 2. Amide-Related Tautomerization Process in H_3L1 (with the Tautomers' Percentages at Equilibrium) and the Labeling System Employed for the Assignment of the NMR Data According to the XRD Numbering Scheme

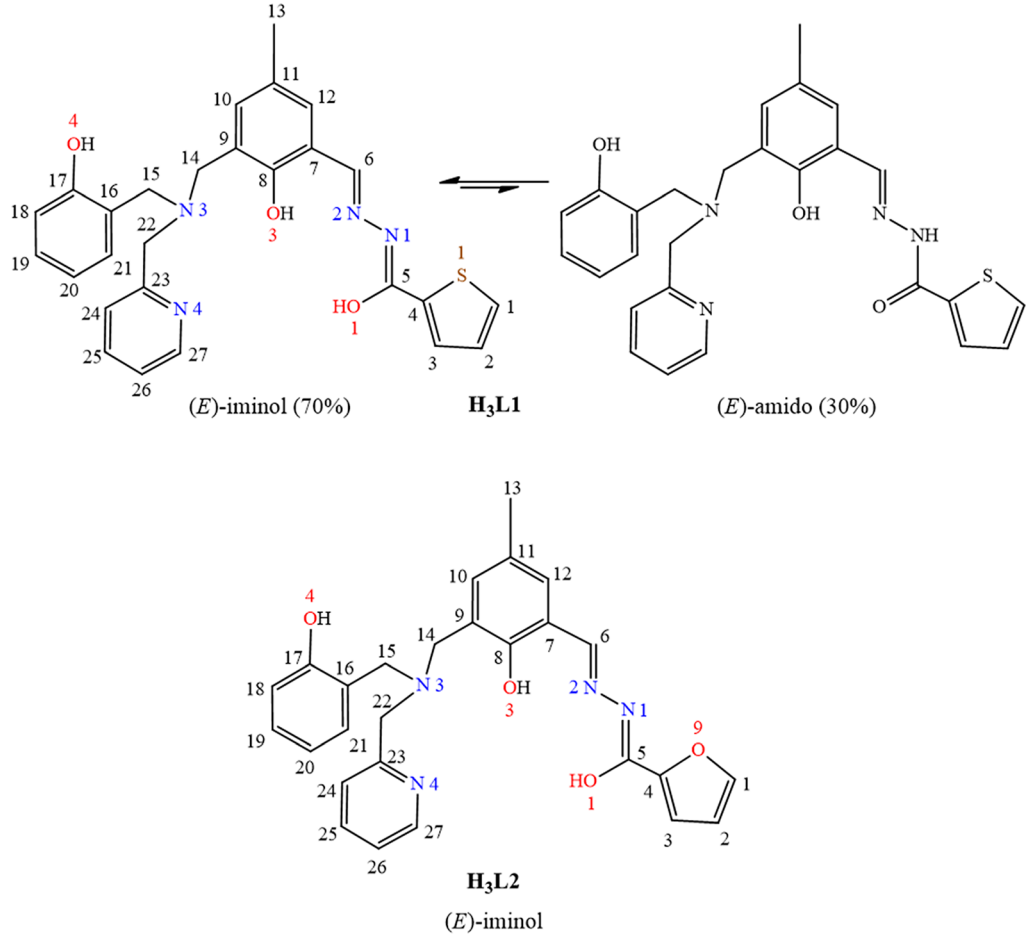

tautomers (Scheme 2). Because in the ^{13}C NMR spectrum of this ligand the carbonyl signal at 161.04 ppm is not part of the main set, we suggest that the iminol form constitutes the predominating species. This is expected because the tautomer is stabilized by intramolecular hydrogen bonding between O1−H and N2. In contrast, **H_3L2** does not show any duplicated signal and, thus, exists in just one tautomeric form. The absence of the carbonyl resonance above 160 ppm represents supporting evidence that, for both ligands, the same species prevail at equilibrium. Because iminol [−(HO)C═NN═C−] seems to be much more stable in solution for these systems, the present NMR analysis focuses only on this tautomer.

A complete assignment of the hydrogen and carbon nuclei for the new ligands **H_3L1** and **H_3L2** is reported (Table S1). The chemical shifts previously published by our research group for the precursor HBPAMFF were employed as a starting point for the assignment of the nonhydrazonic moiety of the ligands.[52] 2D COSY maps helped us to confirm the identity of aromatic hydrogen nuclei because some signals appear to be overlapped and, in the case of **H_3L1**, duplicated because of the iminol/amide tautomerism. As expected, the ^1H and ^{13}C NMR spectra of **H_3L2** are very similar to those of **H_3L1** except for the absence of tautomeric equilibrium in the former under the conditions of the present study.

ESI-MS Analysis of the Ligands. Two prominent peaks were observed at m/z^+ 509 and 995 for **H_3L1** and at m/z^+ 493 and 963 for **H_3L2**. These peaks were assigned, respectively, to the sodium-associated monomeric and dimeric species $[\mathbf{H_3L} + Na^+]^+$ and $[(\mathbf{H_3L})_2 + Na^+]^+$.

Crystal Structures of 1 and 2. Figure 1 shows the structures of the cationic complexes present in **1** and **2**. Selected bond distances and angles are listed in Table 1. Detailed crystal data, collection, and refinement parameters can be found in Tables S2 and S4.

The crystal structures indicate that both complexes generate dimeric arrangements containing two partially deprotonated ($\mathbf{HL1}^{2-}$ or $\mathbf{HL2}^{2-}$) ligands and four divalent copper centers. In fact, compounds **1** and **2** are quite similar, exhibiting two crystallographically independent metal sites (Cu1 and Cu2) with intermetallic distances of 2.944 and 2.923 Å, respectively. Cu1, which is coordinated by the hydrazonic moiety of the ligand, comprising the donor atoms N2 and O1 (corresponding to the iminolate form), shows a square-planar geometry with a slightly distorted plane [the average distances among the atoms and the best plane are 0.012(4) and 0.03(1) Å, correspondingly, for complexes **1** and **2**]. Endogenous (O3) phenoxo and exogenous (O2) hydroxo bridges complete the coordination sphere. On the other hand, Cu2 exhibits an N_2O_4-type octahedral environment distorted by a pronounced Jahn−Teller effect. The equatorial plane contains the tertiary amine N3 and the pyridine N2 atoms, in addition to the O3 phenoxo and O2 hydroxo bridges. The apical positions are occupied by the protonated phenol oxygen O4 and by the

DOI: 10.1021/acs.inorgchem.9b01195
Inorg. Chem. XXXX, XXX, XXX−XXX

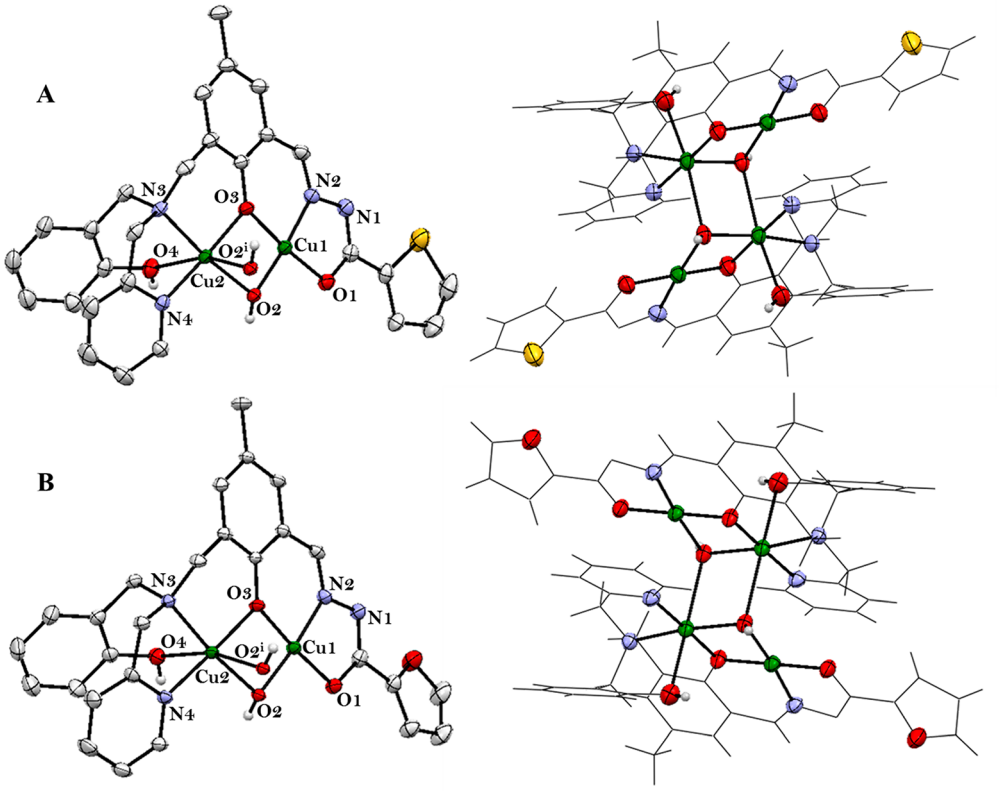

Figure 1. (Left) Crystal structure representations of **1** (A) and **2** (B). The ellipsoids were drawn with 30% probability. Only one of the enantiomers is shown. Perchlorate counterions, disordered water molecules, and most of the hydrogen atoms were omitted for the sake of clarity. Symmetry code: (i) $-x + 1, -y + 1, -z + 1$. (Right) Corresponding dimers, formed by a pair of enantiomers interacting through trifurcated hydroxo bridges (O2- and $O2^i$-donor atoms), with the copper(II) coordination spheres highlighted as colored ellipsoids.

bridging hydroxo $O2^i$ atom of another dinuclear unit, constituting a nice example of a trifurcated bridge, with the structural function of maintaining the dimer's integrity. When the compounds are in solution, those interactions are probably disrupted, and Cu2 should assume a square-pyramidal geometry. The furan and thiophene rings are not involved in coordination.

Two perchlorate counterions, located in voids, were also observed in the crystal lattice for each complex dimer. Dimers present moderate O···O hydrogen bonds between both the terminal endogenous (O4) and bridging exogenous (O2) hydroxides and the perchlorate counterions. The crystal packing is also stabilized by weak CH···O interactions involving perchlorate and methylene groups. Moreover, for complex **1**, CH···S interactions between the ligands could be identified also. A complete list of the hydrogen-bonding geometries present in complexes **1** and **2** can be found in Tables S3 and S5, respectively.

Vibrational Properties of the Compounds. Both H_3L1 and H_3L2 and their corresponding dicopper(II) complexes **1** and **2** were studied under the perspective of vibrational (IR and Raman) spectroscopy. All of the spectra are available in Figures S10–S15, where the IR spectrum of the HBPAMFF precursor (Figure S9) is also included. When the vibrational bands of the free ligands are compared to those of their metal compounds (Figures S10 and S11), clear signs of complexation are evidenced. Probably, the most patented among them are related to deprotonation of the hydrazonic group upon coordination. For example, in the IR spectrum of H_3L1, the NH stretching mode is observed at 3151 cm^{-1}, and the band at 1555 cm^{-1} is assigned to the amide N–H bending vibration. In the TCH precursor, this mode appears at 1542 cm^{-1}.[74] The complete absence of these bands in the FTIR spectrum of **1**, as well as the pronounced shift of the $\nu_{C=O}$ band to lower wavenumbers, indicates that the ligand loses the amide hydrogen atom and is coordinated in its iminolate form, which is in agreement with the acidic nature of this group and the use of stoichiometric sodium hydroxide during the last step of the complexes' syntheses.

As expected, specific bands for the perchlorate counterions are also present in the vibrational spectra of complexes **1** and **2**. The main vibrational frequencies of H_3L1, H_3L2, and their coordination compounds, along with the proposed assignments, are summarized in Table S6.

UV–Visible Spectroscopy Studies of the Compounds. Both H_3L1 and H_3L2 display five foremost absorptions in the 250–500 nm spectral range, as shown in Figure 2 (top), in which the spectra of the precursor HBPAMFF and the respective hydrazides are also shown for the sake of comparison. Three of those absorptions are also present in the precursors and are probably related to the thiophene/furan and HBPAMFF transitions.

The most intense UV bands occur at 312 nm (H_3L1) and 310 nm (H_3L2), followed by strong absorptions centered at 300 nm (H_3L1) and 298 nm (H_3L2), corresponding to the aroylhydrazone transitions, because they are completely absent in the spectra of the precursors. The upper half of Table S7 displays the absorption bands of both ligands along with their respective molar absorptivity coefficients and suggested assignments.

DOI: 10.1021/acs.inorgchem.9b01195
Inorg. Chem. XXXX, XXX, XXX–XXX

Table 1. Selected Geometric Parameters for Complexes 1 and 2[a]

	1	2
	Bond Distances (Å)	
Cu1−O1	1.910(1)	1.895(2)
Cu1−O2	1.933(1)	1.924(2)
Cu1−O3	1.914(1)	1.908(2)
Cu1−N2	1.911(2)	1.905(2)
Cu2−O2	1.952(1)	1.949(2)
Cu2−O3	1.960(1)	1.956(2)
Cu2−O4	2.574(2)	2.570(2)
Cu2−N3	2.005(2)	2.003(2)
Cu2−N4	1.984(2)	1.976(2)
Cu2−O2^{i}	2.599(2)	2.590(2)
	Bond Angles (deg)	
Cu1−O2−Cu2	98.49(6)	97.99(9)
Cu1−O3−Cu2	98.90(6)	98.32(9)
O1−Cu1−O2	103.49(6)	102.05(9)
O1−Cu1−O3	175.23(6)	175.67(10)
O1−Cu1−N2	82.46(7)	83.06(10)
O2−Cu1−O3	80.89(5)	81.54(8)
O2−Cu1−N2	174.02(6)	174.72(10)
O3−Cu1−N2	93.14(7)	93.42(10)
O2−Cu2−O3	79.25(6)	79.69(8)
O2−Cu2−N3	171.01(6)	171.60(9)
O2−Cu2−N4	103.26(6)	102.72(9)
O2−Cu2−O2^{i}	85.79(6)	82.11(9)
O3−Cu2−O4	97.38(8)	97.48(9)
O3−Cu2−N3	92.15(6)	92.20(9)
O3−Cu2−N4	177.48(6)	177.43(9)
O4−Cu2−N3	86.59(7)	86.42(9)
O4−Cu2−N4	81.36(7)	83.39(9)
N3−Cu2−N4	85.37(7)	85.43(10)

[a]Symmetry code: (i) $-x + 1, -y + 1, -z + 1$.

The absorption profiles of the complexes are very similar to those of their respective ligands. Nevertheless, the bands related to the hydrazone group and to the HBPAMFF-derived central phenol system are bathochromically shifted in the spectra of **1** and **2** (Figure 2, bottom). The presence of the iminolate tautomeric form in the complexes, as well as deprotonation of the central (bridging) phenol group upon coordination, increases electron delocalization all over this moiety of the ligand. In both complexes, a broad low-intensity (Table S7, lower half) absorption is also observed from 550 to 800 nm. These bands, centered at 667 nm for both **1** and **2**, are attributed to d−d transitions between the electronic states of the copper centers. The presence of charge-transfer bands can certainly not be ruled out, although their observation may be impaired because of overlap with the intraligand absorptions.

Hydrolysis Studies. Substances containing the hydrazone group are known to be prone to dissociate into the respective carbonyl compound and hydrazide in water. However, an aqueous medium is necessary for most biological tests and, even more significant, water constitutes the universal physiological solvent. For this reason, the stabilities of the ligands and complexes were monitored by UV−visible, over 24 h, in water solutions containing 10% DMSO to ensure for complete dissolution of the compounds. The hydrazone-related bands at 312/299 nm (H_3L1), 308/299 nm (H_3L2), 343/330 nm (**1**), and 333/320 nm (**2**) were used as references. Notice that, in this medium, the ligand and complex absorptions are slightly shifted.

Stability of the Ligands. Over the first 12 h of assay, the absorptions of the ligands' solutions decrease by around 90% (Figure S16). With time, the bands associated with the hydrazone group remain in the same position. However, the wavelenghts from the HBPAMFF-related absorptions are slightly blue-shifted for both ligands, approaching that of the free HBPAMFF precursor. This absorption band of HBPAMFF, at about 340 nm, has a molar absorptivity that is around one-third of those related to the associated bands in H_3L1 and H_3L2. Therefore, our results suggest that, in aqueous solution, the ligands are hydrolyzed in a relatively fast way. The ligands were also assayed in pure (100%) DMSO and in 10% DMSO/90% phosphate-buffered saline (PBS; pH 7.4). In the organic medium, both H_3L1 and H_3L2 demonstrate a remarkable stability, keeping more than 90% of the initial absorbance values during the 24 h of monitoring at room temperature. Although not as stable as in pure DMSO, the ligands are more resistant to hydrolysis in the "buffered" medium than in 10% DMSO/90% water. The initial absorbance value decrease for H_3L1 was only 31% over 24 h, while that for H_3L2 was 63% under the same experimental conditions, as can be observed in Figure S17A,B.

Stability of the Complexes. Over 24 h, both complexes' solutions in 10% DMSO contain 85% (**1**) and 91% (**2**) of their initial absorbances (Figure S18) and, in this sense, are quite resistant to dissociation. Because hydrolysis of the hydrazones begins with protonation of the azomethine nitrogen atom, coordination through this donor atom should prevent that reaction. Upon dissolution in a 10% DMSO/90% PBS (pH 7.4) medium, the stabilities of complexes **1** and **2** remain relatively unchanged (Figure S17C,D). The structural integrity of the complexes in aqueous solution, up to 24 h at room temperature (23 ± 2 °C), was confirmed by ESI-MS analyses (Figure 3). DMSO/water (1:9) stock solution aliquots were analyzed immediately and after 24 h, by direct infusion, after a previous dilution in MeOH (5:95). The MS spectra of both complexes are similar, with three main peaks at m/z^+ 611, 625, and 671 for **1** and m/z^+ 627, 641, and 687 for **2**, which were assigned respectively to the species $[Cu_2(HL)(OH)]^+$, $[Cu_2(HL)(CH_3O)]^+$, and $[Cu_2(L)(DMSO)]^+$, the latter without any exogenous bridging group between the copper(II) ions. In the specific case of complex **1**, additional peaks at m/z^+ 663 and 741 were also observed in the spectrum after 24 h of aging and attributed to the species $[Cu_2(HL)(OH)(OH_2)_2]^+$ and $[Cu_2(HL)(OH)(OH_2)_2(DMSO)]^+$. All of the discussed assignments were supported by comparisons between the experimental and simulated isotopic patterns (Figure S19). No evidence for the dissociation or hydrolysis of coordinated ligands was found. In this sense and considering that the species $[Cu_2(HL)(CH_3O)]^+$ constitutes an "artefact" because of the presence of MeOH used in the dilutions for ESI-MS measurements, we can conclude that, under the experimental conditions employed in the biological assays described below, the main metal-containing species present should be the dinuclear cations themselves characterized by XRD, $[Cu_2(HL)(OH)]^+$, and the DMSO-substituted derivative $[Cu_2(L)(DMSO)]^+$, in which the μ-hydroxo bridge is replaced by a terminal solvent molecule.

Evaluation of BSA Binding through UV−Visible and Fluorescence Spectroscopies. Because of the importance of serum albumin in the transportation of drugs in vertebrates,

DOI: 10.1021/acs.inorgchem.9b01195
Inorg. Chem. XXXX, XXX, XXX−XXX

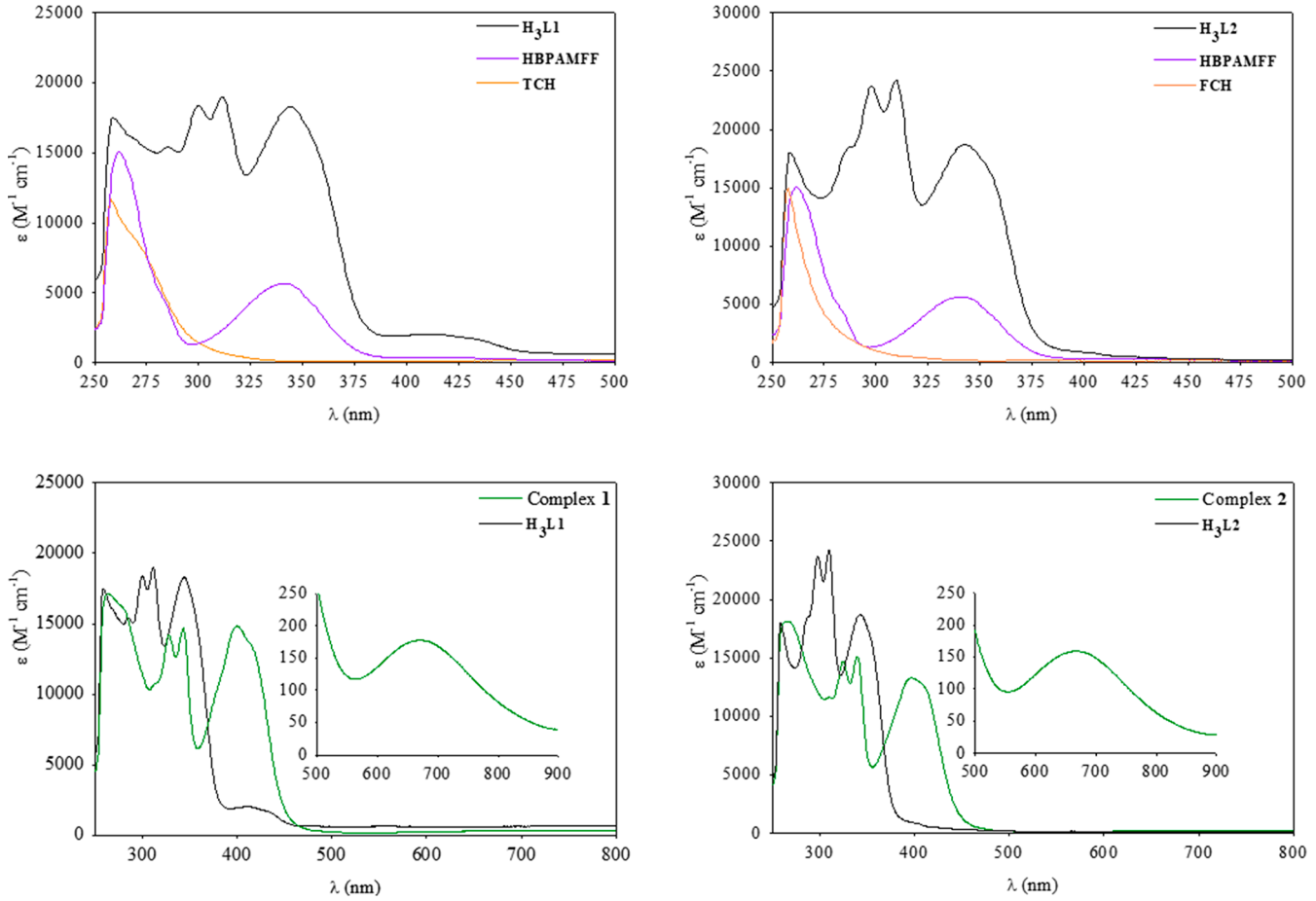

Figure 2. (Top) UV−visible spectra of the ligands $\mathbf{H_3L1}$ (left, 4.6×10^{-5} M) and $\mathbf{H_3L2}$ (right, 4.8×10^{-5} M), as well as their respective precursors HBPAMFF (10.6×10^{-5} M), TCH (7.0×10^{-5} M), and FCH (4.0×10^{-5} M), in DMSO at room temperature. (Bottom) UV−visible spectra of complexes **1** (left, 6.2×10^{-5} M) and **2** (right, 7.0×10^{-5} M) recorded in DMSO at room temperature. The spectra of $\mathbf{H_3L1}$ (3.4×10^{-5} M) and $\mathbf{H_3L2}$ (2.9×10^{-5} M) are included for the sake of comparison. Insets: Visible absorbance of **1** (5.0×10^{-3} M) and **2** (5.0×10^{-3} M) in the 500−900 nm region.

this class of proteins has been extensively studied, as well as their interaction with potential pharmacological agents, including organic ligands and coordination complexes. The bovine-variant BSA presents chemical properties similar to those of human serum albumin[75] (HSA), with only a few differences.[76] Thus, BSA has been largely used as a model in order to study the interactions with many compounds, including copper complexes.[18,77−80] These complexes are well-known by their BSA binding propensity, showing a strong affinity for the protein.[81−84] In recent studies, authors evaluated the interactions of both HSA and BSA with copper(II) complexes. The values found for the binding constants, as well as for the number of binding sites, are in agreement,[85−88] although exceptions, such as the work of Manna and co-workers,[89] were identified.

UV−visible spectroscopy is a common and useful technique to study the structural changes of albumin proteins.[15,90] In the presence of complexes **1** and **2**, the absorption band at 205 nm, related to the peptide bonds of the protein,[91] is red-shifted and an intense absorption decrease is observed (Figure 4A). This hypochromic effect is probably due to the induced perturbation of BSA α helices by the complexes, while the shift toward longer wavelengths is produced by the changes in the polarities of their surroundings.[92] BSA presents similar spectral changes for this absorption in the presence of free ligands (Figure 4B). The band at 280 nm, on the other hand, is associated with the aromatic amino acids in the protein.[91] Although, upon addition of the copper(II) complexes, its intensity seems to remain unchanged (Figure 4A, inset), this absorption band increases slightly in the presence of the ligands, indicating that the interaction of $\mathbf{H_3L1}$ and $\mathbf{H_3L2}$ with BSA modifies the microenvironments of the residues of their aromatic amino acids.[92]

On the other hand, fluorescence spectroscopy has been widely used as an efficient technique for analysis of the BSA conformational changes and binding with different compounds.[15] Parts C and D of Figure 4 present the effect of copper(II) complexes in the fluorescence emission of BSA. Following the addition of **1** or **2** to a BSA solution, the protein fluorescence intensity at 353 nm gradually decreases when the concentrations of the complexes increase, suggesting that the quenching mechanism is primarily of the static (or contact) type, i.e., through the generation of a protein/complex adduct in the ground state (before excitation). Because of significant absorption of the complex/BSA solutions at the emission wavelength, the fluorescence measurement was treated to correct the "inner filter" effect (eq 1).[93] This equation is limited to solutions with absorbances lower than 0.3.

$$F_{corr} = F_{obs}\ \text{antilog}[(A_{ex} + A_{em})/2] \quad (1)$$

DOI: 10.1021/acs.inorgchem.9b01195
Inorg. Chem. XXXX, XXX, XXX−XXX

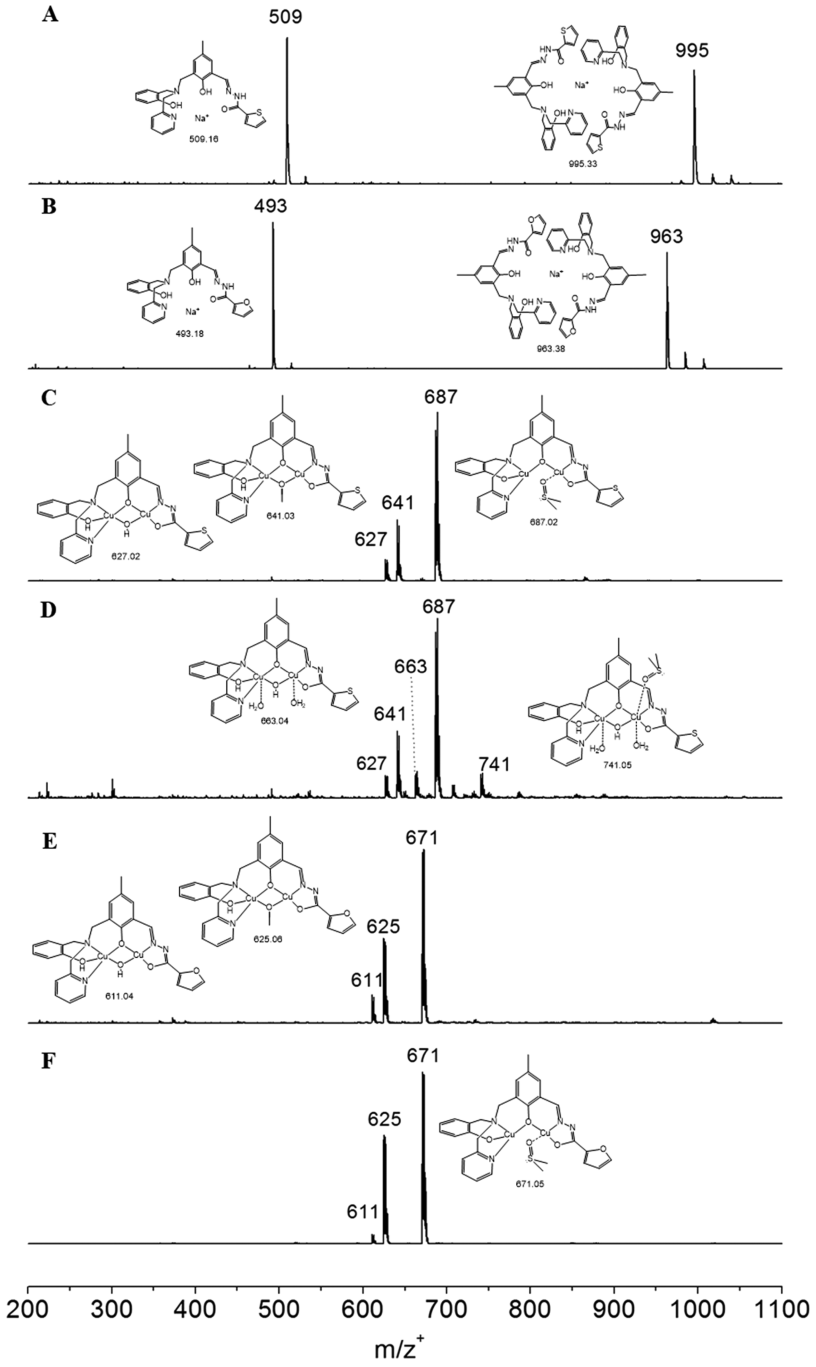

Figure 3. ESI-MS(+) spectra measured from fresh DMSO/MeOH solutions of H_3L1 (A) and H_3L2 (B). (C) Complex **1** in a fresh DMSO/water solution. (D) **1** in a DMSO/water solution after 24 h at 23 ± 2 °C. (E) Complex **2** in a fresh DMSO/water solution. (F) **2** in a DMSO/water solution after 24 h at 23 ± 2 °C. The capillary output voltage was set at 50 V. All compounds were diluted in MeOH (5:95) before injection.

where F_{corr} and F_{obs} are respectively the corrected and measured fluorescence intensities. A_{ex} corresponds to the absorbance value at the excitation wavelength used to acquire the fluorescence spectra and A_{em} to that at the emission wavelength in a 1.0-cm-path-length cuvette. The Stern–Volmer equation (eq2)[94] was used to infer in a more accurate way the main quenching mechanism and to determine the respective constants

$$I_0/I = 1 + K_{SV}[Q] = 1 + K_q\tau_0[Q] \quad (2)$$

where I_0 and I are, correspondingly, the steady-state fluorescence intensities in the absence and presence of the quenching agent. [Q] is the quenching agent concentration, K_q is the biomolecular quenching rate constant, and τ_0 is the average lifetime of the protein in the absence of a quencher, equal to 10^{-8} s.[95] The Stern–Volmer constant for the adduct formation, K_{SV}, can be determined directly from the slope of the straight line obtained when I_0/I versus [Q] is plotted. The K_{SV} and K_q constants for complexes **1** and **2** can be found in Table 2.

The maximum value of the K_q parameter for a mechanism to be considered of a pure dynamic quenching type is 2.0×10^{10} M^{-1} s^{-1}. Complexes **1** and **2** presented K_q values of about 3 order of magnitude higher than that expected for a diffusion-

DOI: 10.1021/acs.inorgchem.9b01195
Inorg. Chem. XXXX, XXX, XXX–XXX

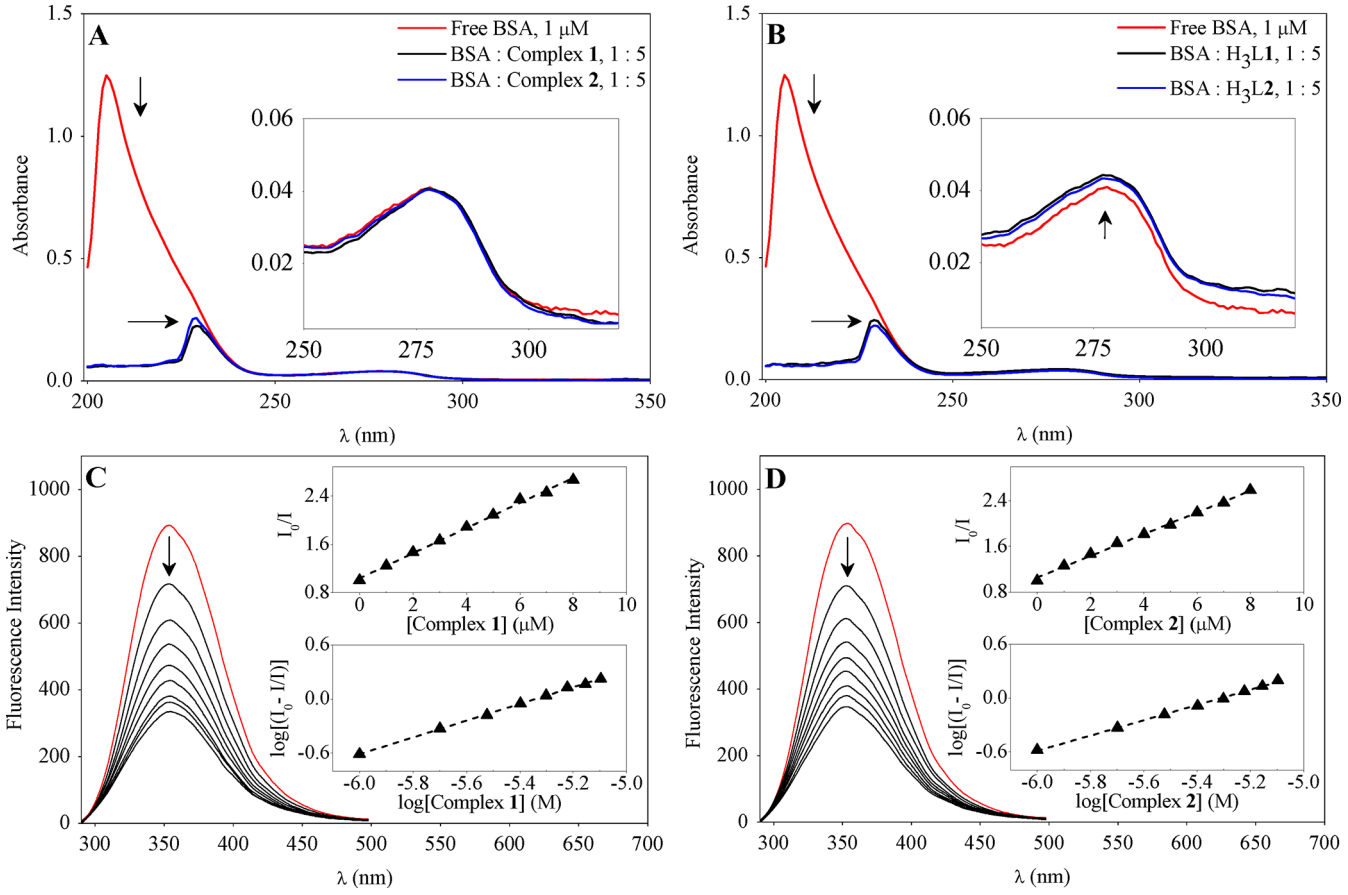

Figure 4. UV−visible spectra of the BSA (1 μM) in a buffer solution (10 mM Tris-HCl and 10 mM NaCl at pH 7.40) in the absence and presence of the complexes (A) and ligands (B) at a 5 μM concentration. Insets: Details of the 250−320 nm region. Fluorescence spectra, at 25 °C, of BSA (1 μM; λ_{ex} = 280 nm; λ_{em} = 353 nm) in the absence (red curve) and presence (black curves) of increasing concentrations (1−8 μM) of the dicopper(II) complexes **1** (C) and **2**(D). Insets: Corresponding Stern−Volmer and Scatchard plots.

Table 2. Quenching and Binding Parameters for the Interaction of Complexes 1 and 2 with BSA at 25 °C

compound	K_{SV} ($\times 10^5$ M^{-1})	K_q ($\times 10^{13}$ M^{-1} s^{-1})	K_b ($\times 10^4$ M^{-1})	n
1	2.08 ± 0.04	2.08	9.23	0.93
2	1.90 ± 0.04	1.90	3.29	0.85

controlled fluorescence quenching,[92] indicating that the systems under study are dominated by a static quenching mechanism, caused by the interaction between BSA and the complexes.

To determine the binding constants, K_b, and the number of complexes bound to each BSA unit, n, the Scatchard equation was employed (eq 3).[96]

$$\log[(I_0 - I)/I] = \log K_b + n \log [Q] \quad (3)$$

In the linear fit plot of eq 3, the intercept corresponds to log K_b and the slope to n.

The calculated protein binding constants (Table 2) are 9.23 × 10^4 M^{-1} and 3.29 × 10^4 M^{-1} for complexes **1** and **2**, respectively. Therefore, the affinity of **1** for BSA is 2.8 times higher than that of **2**. The K_b values found are perfectly comparable to those obtained for the interaction of BSA with previously reported copper(II) complexes.[77] The calculated n parameter indicates a single binding site in BSA for the complexes.

Influence of the Compounds in BSA Conformation by Scattering Techniques. Scattering techniques have recently been used as an alternative tool to other spectroscopic methods for characterizing the structures formed due to the interaction between different compounds and BSA.[97−102] Figure 5 presents the size distributions of BSA before and after the addition of different concentrations of **1** and **2**. The corresponding autocorrelation functions are presented in Figure S20. Native BSA has only one population with a hydrodynamic diameter of 8.6 ± 0.1 nm. Both the ligands and complexes are too small to be detected by DLS and do not exhibit significant scattering intensity. Upon the addition of **1**, the diameter gradually increases by up to 18 nm and a new population of larger particles (from 133 to 225 nm) are observed, which are probably related to the formation of aggregates. Nonfiltered compound/BSA samples, i.e., preserving the whole spectrum of the particles' sizes, were also analyzed and indicate that the addition of **1** to BSA solutions leads to the formation of another population of aggregates larger than 1 μm (which are not adequate to be precisely characterized by DLS because they present a high scattering intensity, making the samples more turbid). Similar trends were observed for **2** and ligands **H_3L1** and **H_3L2**, as is also shown in Figures 5 and S20. However, ligands caused a minor change in the hydrodynamic size of BSA compared with their respective complexes under the same conditions (BSA/compound molar ratio of 1:28). The obtained results indicate

DOI: 10.1021/acs.inorgchem.9b01195
Inorg. Chem. XXXX, XXX, XXX−XXX

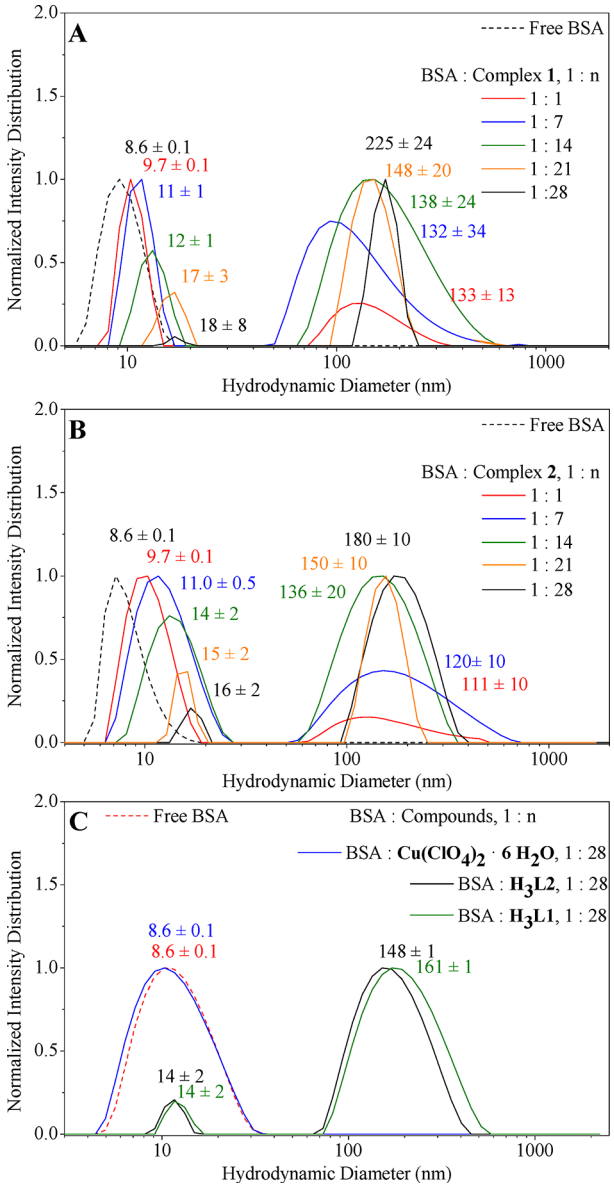

Figure 5. Hydrodynamic diameter (nm) distribution, at 25 °C, of BSA samples (5×10^{-5} M) in the absence and presence of complexes **1** (A) and **2** (B) at BSA/complex molar ratios of 1:1, 1:7, 1:14, 1:21, and 1:28. (C) BSA in the absence and presence of $Cu(ClO_4)_2 \cdot 6H_2O$ and free ligands H_3L1 and H_3L2 at a BSA/compound molar ratio equal to 1:28. Scattering angle: 90°. Samples (2 mL, in 100 mM NaCl and 50 mM Tris buffer at pH 7.40) were filtered (0.25 μm) before the scattering measurements were performed.

that interactions of the ligands and especially the complexes with BSA cause its aggregation. Although the increment in the size of the first population is not significant to evidence the occurrence of conformational changes in the secondary structure of BSA, the obtained values agree with the results from the literature. By DLS measurements, Adel and co-workers[103] reported a hydrodynamic radius for BSA of 3.8 ± 0.2 nm, whereas Yu and collaborators[101] obtained a 7.13 nm hydrodynamic diameter for this protein. In the same direction, Zocchi reported a value of 8 nm for the native BSA hydrodynamic diameter, using micromechanical measurements.[104] Also in accordance with our data, Li and colleagues[100] observed that the addition of an organic compound (pterodontic acid) leads to an increase of the hydrodynamic diameter of BSA from 7.3 to 22.8 nm and to the arising of a second population of larger particles.

Over time, the frequency of the first BSA population (nonaggregated) increases, while the frequency of the population corresponding to aggregated BSA decreases. This observation indicates that aggregation is reversible and could be related to a trend of release of the copper complexes with time and return of the protein to its native form. A comparison between the frequencies of BSA populations in the presence of **1** and **2** after an incubation period of 24 h shows that the protein disaggregates faster for complex **2** than for complex **1**. This behavior could be expected based on the value for the binding constant obtained by fluorescence spectroscopy, which is lower for complex **2** than for complex **1**.

To better evaluate the conformational changes of BSA, SAXS can complement DLS because X-rays have a shorter wavelength than the visible light and are more adequate for evaluating smaller dimensions. Figure 6 presents the

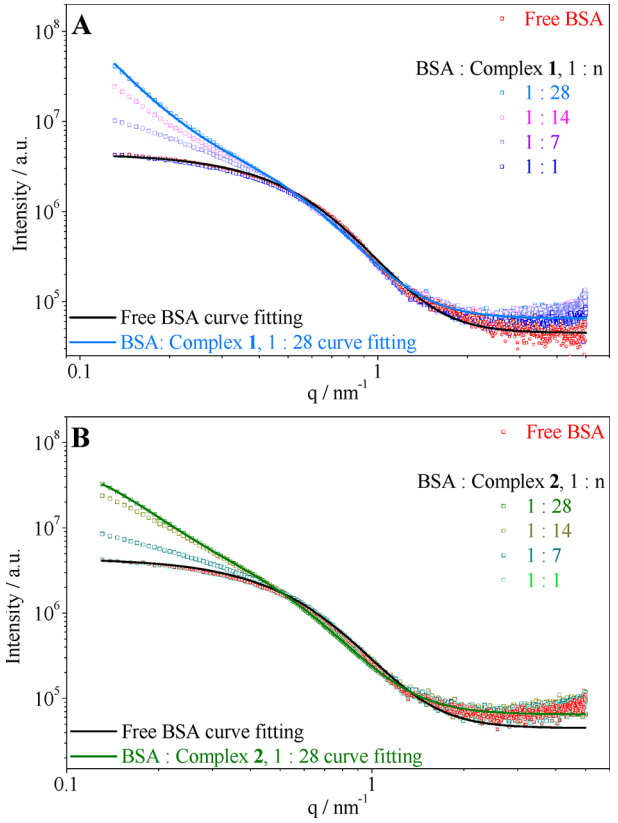

Figure 6. SAXS curves, at 25 °C, of free BSA (5×10^{-5} M, in 100 mM NaCl and 50 mM Tris buffer at pH 7.40) in the absence and presence of complexes **1** (A) and **2** (B) at BSA/complex molar ratios of 1:1, 1:7, 1:14, 1:21, and 1:28. All samples were filtered (0.45 μm) before the scattering measurements were performed. The curve fittings, using a Generalized Gaussian Coil model, for free BSA and BSA/complexes at 1:28 are included.

experimental curves of the scattering intensity, I, as a function of the scattering vector, q, obtained for samples containing BSA and different concentrations of **1** and **2**. Samples containing only the complexes do not present significant scattering intensity. The fitted curve corresponding to the solution of free BSA provided a gyration radius, R_g, of 3.5 nm. Upon the addition of complexes, the intensity is increased in

DOI: 10.1021/acs.inorgchem.9b01195
Inorg. Chem. XXXX, XXX, XXX−XXX

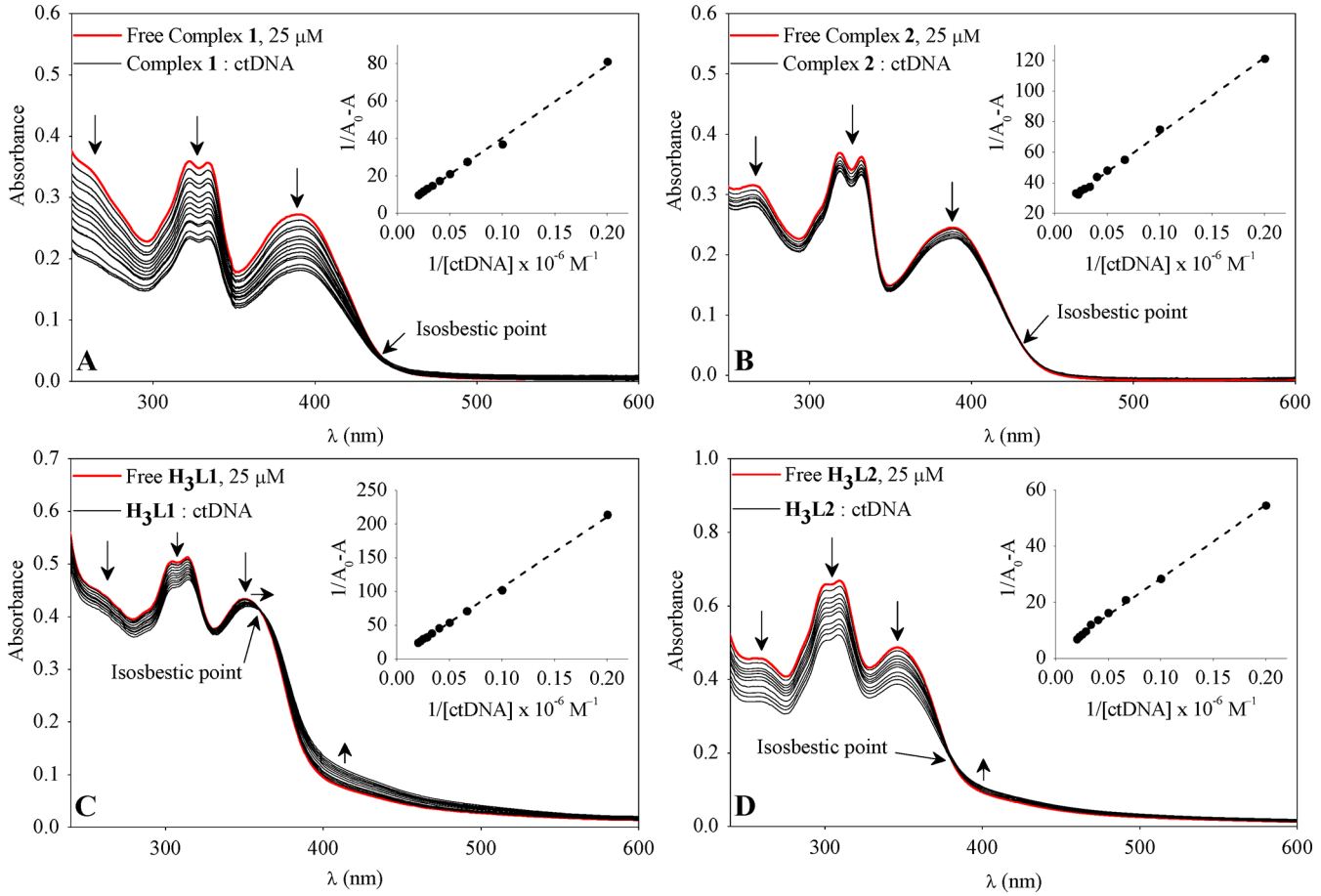

Figure 7. Absorption spectra and $1/(A_0 - A)$ versus 1/[DNA] plots (insets) of the copper(II) complexes **1** (A) and **2** (B) and the ligands H_3L1 (C) and H_3L2(D) (25 μM, 3 mL, in 10% DMSO and 90% 50 mM Tris-HCl, pH 7.40) in the absence (red curve) and with increasing concentrations (black curves) of ctDNA (5−50 μM) at 25 °C. Spectra were registered after an incubation time of 3 min from each ctDNA addition.

the low-q region but is not affected in the high-q region. This indicates that the form factor of BSA is not significantly affected by the presence of the complexes, although there is an aggregation generating larger particles. The samples with higher concentrations of complexes were also fitted considering the existence of two populations. The best fitting resulted in R_g values of 3.8 and 68 nm for **1** and 3.9 and 52 nm for **2**. However, the size of the second population is too large for the available q region, and one can only affirm that there are aggregates with $R_g \geq 68$ nm (**1**/BSA system) and 52 nm (**2**/BSA system). The dimensions of the protein after the addition of the complexes are only slightly bigger (3.8 and 3.9 nm for **1** and **2**, respectively) than those of free BSA. Once more, the results indicate that there is no significant change in size, which could evidence conformational changes on the secondary structure. Yet, the interaction between the complexes and BSA also induces a process of aggregation, confirming the results obtained by DLS. For the sake of comparison, the copper salt $Cu(ClO_4)_2{\cdot}6H_2O$ itself does not induce protein aggregation (Figure S21).

Evaluation of the ctDNA Binding Constant through UV−Visible Spectroscopy. To evaluate the properties of the new compounds as potential anticancer drugs, the study of their interaction with DNA constitutes a significant step in order to better understand the possible mechanism of action involved.[105] Copper(II) complexes have demonstrated a great ability to bind to and cleave DNA.[22,85,106] In the present study, UV−visible spectroscopy was used to investigate the interactions of the synthesized compounds with ctDNA through titration experiments. Upon the addition of increasing amounts ctDNA to solutions containing **1** and **2**, a clear hypochromic effect is observed in the complexes' absorption bands, which suggests an interaction with the biopolymer (Figure 7A,B). Hypochromism is commonly associated with intercalative binding.[98] The free ligands H_3L1 and H_3L2 present a similar behavior in the presence of ctDNA (Figure 7C,D).

The binding constants were determined by monitoring the absorbance bands centered at 322 and 317 nm for complexes **1** and **2**, respectively, as well as those at 314 and 309 nm for the ligands H_3L1 and H_3L2, correspondingly. The treatment of the experimental data was performed by using a modified form of the Benesi−Hildebrand equation (eq 4):[107,108]

$$\frac{1}{A_0 - A} = \frac{1}{\varepsilon_b - \varepsilon_f}\frac{1}{[\text{compound}]_0} + \frac{1}{K_b(\varepsilon_b - \varepsilon_f)}\frac{1}{[\text{compound}]_0}\frac{1}{[\text{DNA}]} \quad (4)$$

where A_0 and A are the absorbance values for the compounds in the absence and presence of DNA, respectively, ε_b and ε_f correspond to the molar absorptivities of the fully bound DNA and of the free compound, correspondingly, $[\text{compound}]_0$ is

DOI: 10.1021/acs.inorgchem.9b01195
Inorg. Chem. XXXX, XXX, XXX−XXX

the initial concentration of the compound, [DNA] is the concentration of added DNA, and K_b is the binding constant. A plot of $1/(A_0 - A)$ versus $1/[DNA]$ gives an intercept equal to $1/(\varepsilon_b - \varepsilon_f) \times 1/[compound]_0$ and a slope equivalent to $1/K_b(\varepsilon_b - \varepsilon_f) \times 1/[compound]_0$. Thus, K_b is determined by the ratio of the intercept to the slope (Figure 7A–D, insets). The calculated binding constants for complexes **1** and **2** are $(3.50 \pm 0.08) \times 10^3$ and $(4.38 \pm 0.08) \times 10^4$ M^{-1}, respectively. These values are comparable to those obtained for other reported copper(II) complexes.[98] However, they are lower than the values usually found for representative DNA intercalators, such as ethidium bromide (which is around 10^5–10^6 M^{-1}).[109] This outcome could indicate that intercalation between the base pairs is not the main mode of interaction of the synthesized dicopper(II) complexes with DNA. On the other hand, a binding constant of $(1.64 \pm 0.08) \times 10^3$ M^{-1} was calculated for H_3**L1** and that of $(7.91 \pm 0.08) \times 10^3$ M^{-1} for H_3**L2**.

According to the binding results, complex **2** presents a higher affinity than complex **1** toward ctDNA, a trend also observed with H_3**L2** in comparison to that with H_3**L1**. The free ligands showed a minor intercalator ability compared to that of their respective dinuclear complexes, which is in agreement with the results previously reported for other aroylhydrazones and their copper(II) complexes.[9] The lower intercalative affinity of **1** could be related to its higher reactivity toward DMSO, as shown by ESI-MS(+) measurements, because the DMSO-substituted species should present an impaired planarity regarding the intercalative moiety constituted by the central phenol ring and the aroylhydrazone-derived pendant arm. As mentioned above, the experimental data indicate that coordination to copper(II) increases the binding affinity for DNA.

Influence of the Compounds in a pBR322 Plasmid DNA Conformation by DLS. In many previous reports, both mononuclear and dinuclear copper(II) complexes have shown cleavage activity on plasmid DNA.[6,28,110–112] The effects of cleavage agents over plasmids, leading to their transition from supercoiled (form I) to circular (form II) to linear (form III) conformations of DNA, have been largely studied by gel and capillary electrophoresis. Recently, however, scattering techniques have their importance increased in this context.[113]

In this work, DLS measurements were also used to evaluate the influence of the synthesized compounds in a pBR322 plasmid DNA conformation. To carry out these studies, it was not possible to use SAXS because the samples do not present significant X-ray scattering in this range of concentrations. Solutions of pure native plasmid DNA were not detected by DLS as well, probably because of the absence of sufficient contrast.

Figure 8 presents the size distributions of DNA macromolecules in aqueous solutions with different concentrations of complexes **1** (A) and **2** (B). Figure S22 presents the corresponding autocorrelation functions. When complexes are added to the pBR322 DNA solutions, a population is observed with mean hydrodynamic radii of 58 ± 4 and 73 ± 6 nm for **1** (10 μM) and **2** (15 μM), respectively. We attribute this population to the plasmid form I. In previous static light scattering studies, the gyration radii (R_g) of different plasmid DNAs have been measured.[114] From these results, the expected radii of pBR322 plasmids, used in the present work, can be estimated by extrapolation (Figure S23) as 89 nm for form I, 124 nm for form II, and 171 nm for form III. Upon analysis of the observed radii, it is possible to infer that, at low

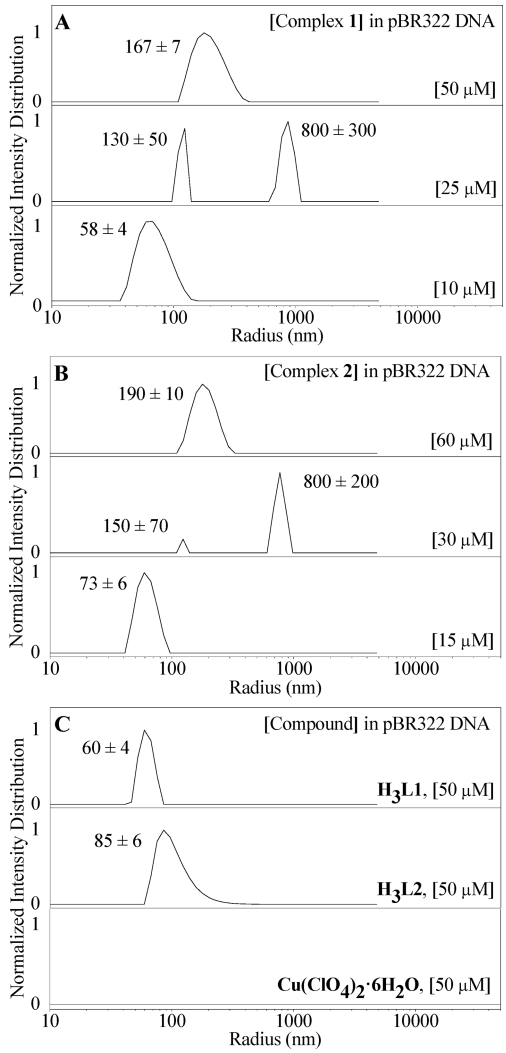

Figure 8. Hydrodynamic radius (nm) distribution of pBR322 plasmid DNA samples (2.5 μg mL^{-1}, 2 mL, in 10 mM Tris buffer, pH 7.40) in the presence of (A) complex **1** (10–50 μM) and (B) complex **2** (15–60 μM). (C) pBR322 plasmid DNA in the presence of H_3**L1**, H_3**L2**, and the starting salt $Cu(ClO_4)_2 \cdot 6H_2O$, all of them at a concentration of 50 μM. Scattering angle: 90°. Incubation: 15 min at 25.0 ± 0.1 °C.

concentrations of the tested complexes (up to 10 μM for **1** and 15 μM for **2**), the interaction is not strong enough to alter dramatically the conformational structure of pBR322 plasmids. Nevertheless, taking into account that the free plasmid had not been detected because of the low contrast of its solution, it is deduced that the complexes interact with plasmids, causing a significant increase in their contrast, which allowed the autocorrelation functions to be obtained. The observed differences between the hydrodynamic radius of plasmid form I in the presence of the complexes and the free plasmid gyration radius estimated by extrapolation is possibly due to an electrostatic interaction between the positively charged dicopper(II) complexes and the negatively charged phosphate groups of pBR322, which can be responsible for DNA compaction[115] in the solutions containing **1** and **2**.

The further addition of **1** (25 μM) or **2** (30 μM) caused a significant increase in the plasmid hydrodynamic radius to 130 ± 50 or 150 ± 70 nm, respectively. The obtained values are similar to those estimated for the circular plasmid form II (~125 nm). However, the generation of a second population

DOI: 10.1021/acs.inorgchem.9b01195
Inorg. Chem. XXXX, XXX, XXX–XXX

Table 3. Growth Inhibition, Expressed as $IC_{50} \pm SD$, of Several Cancer Cell Lines [HCT116 (Colon, Human), HT29 (Colon, Human), MDA-MB-231 (Breast, Human), and B16F10 (Melanoma, Mouse)] after Incubation for 36 h in the Presence of the Synthesized Compounds[a]

	H_3L1		1		H_3L2		2	
cell line	IC_{50} (μM)	SI	IC_{50} (μM)	SI	IC_{50} (μM)	SI	IC_{50} (μM)	SI
HCT116	2.97 ± 0.54	2.90	**0.56 ± 0.55**	1.16	5.17 ± 0.12	2.84	1.42 ± 0.53	1.73
HT29	2.09 ± 0.36	4.12	**0.78 ± 0.47**	0.83	4.20 ± 0.42	3.5	1.89 ± 0.48	1.30
MDA-MB-231	1.02 ± 0.24	8.45	**0.90 ± 0.28**	0.72	**0.65 ± 0.26**	22.6	1.21 ± 0.28	2.03
B16F10	**0.88 ± 0.37**	9.79	**0.32 ± 0.46**	2.03	**0.59 ± 0.72**	24.9	1.23 ± 0.45	2.0
MDCK (control)	8.62 ± 0.34		0.65 ± 0.39		14.7 ± 0.31		2.46 ± 0.38	

[a]The selectivity index (SI) was estimated based on the IC_{50} values obtained for the nontumoral control MDCK cells, also included in the table. The values in bold correspond to those in the submicromolar range.

of larger scattering particles (800 ± 300 and 800 ± 200 nm) is observed as well. These particles could be related to the formation of plasmid aggregates, making it difficult to guarantee the biopolymer form at this point. When plasmid pBR322 is in the presence of higher concentrations of complexes **1** (50 μM) or **2** (60 μM), only one population is observed in each case, with a hydrodynamic radius of 167 ± 7 or 190 ± 10 nm, respectively. A single population indicates that plasmid DNA disaggregates, and the size that observed might indicate the occurrence of cleavage to form III, whose R_g was estimated as ∼170 nm. On the other hand, the free ligands **H_3L1** and **H_3L2** have not shown this property (Figure 8C). It is noteworthy that the starting copper salt $Cu(ClO_4)_2 \cdot 6H_2O$ has been previously reported as being nonactive toward the cleavage of plasmid pBR322 DNA.[112]

DLS measurements were repeated over 1 day, in order to test the particles' stability in the **1**/DNA and **2**/DNA samples containing respectively final concentrations of 50 and 60 μM. After 24 h, no significant changes were observed in the hydrodynamic radii of 167 nm (**1**/DNA) and 190 nm (**2**/DNA), which indicates that the process is, overall, irreversible. The difference between the reversibility of the interactions with BSA and those with DNA is mainly related to the nuclease activity exhibited by the complexes. Although the interactions of **1** and **2** with DNA certainly possess electrostatic and intercalative components, covalent binding involving an oxygen-donor atom from the biopolymer's phosphate diester backbone to one coordinatively unsaturated copper center in the complexes should also be important. This constitutes the first step in the general catalytic mechanism of hydrolysis proposed for artificial bioinspired phosphatases/nucleases displaying bimetallic cores at their active sites. The metal centers in such a class of catalysts usually work cooperatively, and, in this sense, dissimilarities in terms of their coordination spheres could increase the complementarity needed in order to potentialize cooperativity between the metal centers.

A smaller amount of complex **1**, compared to complex **2**, is needed to cause an increase in the hydrodynamic radius of pBR322 plasmid DNA, which is, in fact, the opposite trend observed for their intercalation ability. In general, DLS results indicate that complexes interact more strongly with DNA than their free ligands, as expected based on the binding constants determined by UV−visible spectroscopy. Additionally, the complexes presented the capacity to cleave DNA, which constitutes an assumed mode of action for potential anticancer agents.

Cytotoxic Activity. In order to determine the putative antineoplastic activity of the synthesized compounds, we evaluated the their effect and the effect of their ligands on cell proliferation, using a panel of different cancer cell lines. By performing tetrazolium salt reduction assays, we observed that all of the compounds analyzed effectively decreased the cancer cell proliferation, in vitro, in a dose-dependent manner (data not shown). Indeed, IC_{50} values obtained for all of the tested cell lines fit into the micromolar range, with even some submicromolar values (Table 3). Interestingly, compounds **1** and **2** seemed to be more effective than their respective ligands, affecting the cell proliferation at lower doses. Nevertheless, these complexes showed a decreased selectivity against cancer cells after analysis of their effect on nontumoral cells Madin−Darby canine kidney (MDCK).

The higher antiproliferative effects among the compounds tested are undoubtedly seen for **1**, which is also the most reactive complex regarding plasmid DNA cleavage (as shown by the DLS studies). However, complex **1** is not the one with the highest intercalation affinity because **2** presents a binding constant toward ctDNA 10 times greater than that determined for **1**. Interactions of complexes **1** and **2** with double-stranded DNA seem to involve electrostatic (because both complexes are cationic), intercalative, and coordinative components. Therefore, in such a multifaceted panorama, pointing out the most significant factor for an improved antiproliferative activity is not straightforward. On the other hand, our results suggest that the DNA-damaging capacity is directly related to the cytotoxicity, while a higher binding affinity toward ctDNA seems to be associated with an enhanced selectivity index.

Concerning the ligands, hydrolysis constitutes an aspect to be taken into account, particularly in the case of **H_3L2**. Nevertheless, they also present an interesting antiproliferative profile, with IC_{50} values in the low micromolar range. A possible mechanism for the cytotoxicity exhibited by the ligands could be related to the formation of metal complexes in the culture medium or inside the cells. The compounds thus generated could either be cytotoxic per se, or, alternatively, their formation could deplete the available amount of some physiologically relevant metal ions, such as iron(III). However, additional work would be necessary in order to confirm this hypothesis. What is certain is that the free ligands are much less toxic to the MDCK control cells than the dicopper(II) complexes **1** and **2**.

So, from a medicinal chemistry point of view, ligands **H_3L1** and, especially, **H_3L2** seem to be more promising than their respective metal compounds because of their higher selectivity indexes, particularly in the case of the human breast cell line MDA-MB-231. However, their apparent susceptibility to hydrolysis should impair this performance, although their reversible binding to serum albumin could partially protect

DOI: 10.1021/acs.inorgchem.9b01195
Inorg. Chem. XXXX, XXX, XXX−XXX

them from this undesirable side reaction. On the other hand, the dicopper(II) complexes are much more stable and are also able to bind serum albumin in a reversible manner. Despite their higher intrinsic activity, as mentioned above, they are less selective toward cancer cells (i.e., more toxic for the MDCK control cells). Yet, binding to serum albumin could reduce their toxicity in living systems. A better panorama regarding the real significance of these complexes as anticancer agents can only be obtained after in vivo tests, which are already underway and will be the subject of future reports.

CONCLUSIONS

Two novel C_1-symmetric binucleating ligands comprising hydrazonic moieties and their μ-hydroxo dicopper(II) complexes, **1** and **2**, were synthesized and fully characterized. XRD analyses indicate that both coordination compounds are very similar in structural terms and generate dimeric arrangements containing two partially deprotonated ligands and four divalent copper centers. Although UV−visible measurements indicate that the free ligands are quite susceptible to hydrolysis in a 90% water-containing medium, complexation to copper(II) ions seems to prevent this reaction. The dinuclear metal compounds reported in this work are, indeed, very stable in aqueous solution, concerning both ligand hydrolysis and complex dissociation. ESI-MS(+) analyses confirmed that the main metal-containing species present in a 10% DMSO/water solution should be the dinuclear cations characterized by XRD, $[Cu_2(HL)(OH)]^+$, as well as the DMSO-substituted derivative $[Cu_2(L)(DMSO)]^+$, in which the μ-hydroxo bridge is replaced by a terminal solvent molecule.

Both complexes and ligands show a high affinity for BSA, indicated by the observed static quenching of the protein fluorescence due to interaction with the compounds. Additionally, scattering techniques (DLS and SAXS) suggest that the complexes and their free ligands interact with BSA in a reversible manner. Because BSA is an important protein involved in the transportation of drugs in the biological system, possessing properties similar to those of HSA, the observed results indicate that the new compounds could be targeted through blood transport. The biological activity of the compounds also includes interaction with ctDNA, with the complexes showing a higher affinity than their respective ligands. Moreover, the plasmid pBR322 DNA cleavage results from DLS indicate that the complexes interact electrostatically with plasmid DNA at low concentrations. At the higher concentrations of 50 μM (**1**) or 60 μM (**2**), in contrast, data seem to point to the occurrence of DNA cleavage to form III (linear). Over time, the value of the hydrodynamic radius for plasmid DNA form III remained stable and, therefore, the process is not reversible. Concerning the ability to cause damage to plasmid pBR322 DNA, complex **1** is more active than **2**. Both ligands and their dicopper(II) complexes display potent antiproliferative activity in the cancer cell lines evaluated, occasionally even in the submicromolar range. Once the effect of the metal complexes on tumor cell proliferation was analyzed, it was clear that the addition of copper to the ligands $\mathbf{H_3L1}$ and $\mathbf{H_3L2}$ increased their activity. Our data on the cellular models correlate quite well with the DNA interaction experiments because IC_{50} values are smaller for **1**, which showed the higher activity on DNA by DLS studies. Thus, although the presence of the furan ring seems to be important for an improved DNA intercalation ability (which can involve the formation of anchoring hydrogen bonds between **2** and the biopolymer), the thiophene ring can somehow increase the reactivity of **1** toward DNA. Probably both complexes would be acting at the DNA level, promoting replicative stress or (most likely) cleavage, leading to checkpoint responses and the onset of apoptosis. However, further studies should be addressed to confirm this hypothesis. Finally, the present work shows that aroylhydrazone-derived binucleating ligands and their dinuclear μ-hydroxo dicopper(II) complexes may represent a promising structural starting point for the development of highly active potential antitumor agents.

ASSOCIATED CONTENT

Supporting Information

The Supporting Information is available free of charge on the ACS Publications website at DOI: 10.1021/acs.inorgchem.9b01195.

Optical photographs of ligands' and metal complexes' crystals (Figures S1 and S2), 1D and 2D NMR spectra of the ligands (Figures S3−S8), NMR assignments of the ligands (Table S1), additional crystallographic tables (Tables S2−S5), vibrational spectra of the compounds (Figures S9−S15), selected vibrational and UV−visible absorption properties (Tables S6 and S7), UV−visible stability profiles (Figures S16−S18), ESI-MS(+) experimental and simulated isotopic patterns for the complexes (Figure S19), DLS autocorrelation functions and SAXS curves (Figures S20−S22), and estimation of the different plasmid pBR322 form radii by extrapolation (Figure S23) (PDF)

Accession Codes

CCDC 1851259 and 1851260 contain the supplementary crystallographic data for this paper. These data can be obtained free of charge via www.ccdc.cam.ac.uk/data_request/cif, or by emailing data_request@ccdc.cam.ac.uk, or by contacting The Cambridge Crystallographic Data Centre, 12 Union Road, Cambridge CB2 1EZ, UK; fax: +44 1223 336033.

AUTHOR INFORMATION

Corresponding Author

*E-mail: nicoarey@puc-rio.br.

ORCID

Ana Maria Percebom: 0000-0002-1511-8656

Nicolás A. Rey: 0000-0002-0624-7560

Notes

The authors declare no competing financial interest.

ACKNOWLEDGMENTS

N.A.R. thanks Fundação Carlos Chagas Filho de Amparo à Pesquisa do Estado do Rio de Janeiro (FAPERJ, Brazil) and Conselho Nacional de Desenvolvimento Científico e Tecnológico (CNPq, Brazil) for the research fellowships awarded. This work was financially supported by FAPERJ, FINEP, and FAPEMIG. J.P.R. is grateful to LABSO-Bio Laboratory and to CAPES and CNPq for doctoral fellowships. The authors also acknowledge the Brazilian National Synchrotron Laboratory (LNLS-CNPEM) for SAXS beamtime (SAXS1-20160298), Prof. Ricardo Queiroz Aucélio (Departamento de Química, PUC-Rio, Brazil) for the fluorescence spectroscopy facilities, and Dr. Michèle Salmain (Institut Parisien de Chimie

DOI: 10.1021/acs.inorgchem.9b01195
Inorg. Chem. XXXX, XXX, XXX−XXX

Moléculaire, Université Pierre et Marie Curie, France) for providing the ctDNA sample for the binding studies. The MS measurement time available at Laboratório Multiusuário de Espectrometria de Massas da Universidade Federal Fluminense is also highly appreciated by the authors.

REFERENCES

(1) Rosenberg, B.; Vancamp, L.; Trosko, J. E.; Mansour, V. H. Platinum Compounds: a New Class of Potent Antitumour Agents. *Nature* **1969**, *222*, 385.
(2) Ndagi, U.; Mhlongo, N.; Soliman, M. E. Metal complexes in cancer therapy - an update from drug design perspective. *Drug Des., Dev. Ther.* **2017**, *11*, 599−616.
(3) Wehbe, M.; Leung, A. W. Y.; Abrams, M. J.; Orvig, C.; Bally, M. B. A Perspective - can copper complexes be developed as a novel class of therapeutics? *Dalton Trans.* **2017**, *46* (33), 10758−10773.
(4) Marín-Hernández, A.; Gracia-Mora, I.; Ruiz-Ramírez, L.; Moreno-Sánchez, R. Toxic effects of copper-based antineoplastic drugs (Casiopeinas) on mitochondrial functions. *Biochem. Pharmacol.* **2003**, *65* (12), 1979−89.
(5) Galindo-Murillo, R.; García-Ramos, J. C.; Ruiz-Azuara, L.; Cheatham, T. E.; Cortés-Guzmán, F. Intercalation processes of copper complexes in DNA. *Nucleic Acids Res.* **2015**, *43* (11), 5364−76.
(6) Santini, C.; Pellei, M.; Gandin, V.; Porchia, M.; Tisato, F.; Marzano, C. Advances in Copper Complexes as Anticancer Agents. *Chem. Rev.* **2014**, *114* (1), 815−862.
(7) Paixão, D. A.; Marzano, I. M.; Jaimes, E. H. L.; Pivatto, M.; Campos, D. L.; Pavan, F. R.; Deflon, V. M.; Maia, P. I. d. S.; Da Costa Ferreira, A. M.; Uehara, I. A.; Silva, M. J. B.; Botelho, F. V.; Pereira-Maia, E. C.; Guilardi, S.; Guerra, W. Novel copper(II) complexes with hydrazides and heterocyclic bases: Synthesis, structure and biological studies. *J. Inorg. Biochem.* **2017**, *172*, 138−146.
(8) Pivetta, T.; Valletta, E.; Ferino, G.; Isaia, F.; Pani, A.; Vascellari, S.; Castellano, C.; Demartin, F.; Cabiddu, M. G.; Cadoni, E. Novel coumarins and related copper complexes with biological activity: DNA binding, molecular docking and in vitro antiproliferative activity. *J. Inorg. Biochem.* **2017**, *177*, 101−109.
(9) Ramachandran, E.; Gandin, V.; Bertani, R.; Sgarbossa, P.; Natarajan, K.; Bhuvanesh, N. S. P.; Venzo, A.; Zoleo, A.; Glisenti, A.; Dolmella, A.; Albinati, A.; Marzano, C. Synthesis, characterization and cytotoxic activity of novel copper(II) complexes with aroylhydrazone derivatives of 2-Oxo-1,2-dihydrobenzo[h]quinoline-3-carbaldehyde. *J. Inorg. Biochem.* **2018**, *182*, 18−28.
(10) Venkatachalam, T. K.; Bernhardt, P. V.; Noble, C. J.; Fletcher, N.; Pierens, G. K.; Thurecht, K. J.; Reutens, D. C. Synthesis, characterization and biological activities of semicarbazones and their copper complexes. *J. Inorg. Biochem.* **2016**, *162*, 295−308.
(11) Almeida, J. D. C.; Paixão, D. A.; Marzano, I. M.; Ellena, J.; Pivatto, M.; Lopes, N. P.; Ferreira, A. M. D. C.; Pereira-Maia, E. C.; Guilardi, S.; Guerra, W. Copper(II) complexes with β-diketones and N-donor heterocyclic ligands: Crystal structure, spectral properties, and cytotoxic activity. *Polyhedron* **2015**, *89*, 1−8.
(12) Iglesias, S.; Alvarez, N.; Torre, M. H.; Kremer, E.; Ellena, J.; Ribeiro, R. R.; Barroso, R. P.; Costa-Filho, A. J.; Kramer, M. G.; Facchin, G. Synthesis, structural characterization and cytotoxic activity of ternary copper(II)-dipeptide-phenanthroline complexes. A step towards the development of new copper compounds for the treatment of cancer. *J. Inorg. Biochem.* **2014**, *139*, 117−123.
(13) Massoud, S. S.; Louka, F. R.; Ducharme, G. T.; Fischer, R. C.; Mautner, F. A.; Vančo, J.; Herchel, R.; Dvořák, Z.; Trávníček, Z. Copper(II) complexes based on tripodal pyrazolyl amines: Synthesis, structure, magnetic properties and anticancer activity. *J. Inorg. Biochem.* **2018**, *180*, 39−46.
(14) Loganathan, R.; Ganeshpandian, M.; Bhuvanesh, N. S. P.; Palaniandavar, M.; Muruganantham, A.; Ghosh, S. K.; Riyasdeen, A.; Akbarsha, M. A. DNA and protein binding, double-strand DNA cleavage and cytotoxicity of mixed ligand copper(II) complexes of the antibacterial drug nalidixic acid. *J. Inorg. Biochem.* **2017**, *174*, 1−13.
(15) Hu, J.; Liao, C.; Guo, Y.; Yang, F.; Sang, W.; Zhao, J. A. Copper(II) complexes inducing apoptosis in cancer cells, and demonstrating DNA and HSA interactions. *Polyhedron* **2017**, *132*, 28−38.
(16) Hu, J.; Guo, Y.; Zhao, J. a.; Zhang, J. In vitro antitumor activity of novel benzimidazole-based Cu(II) complexes. *Bioorg. Med. Chem.* **2017**, *25* (20), 5733−5742.
(17) Bykowska, A.; Komarnicka, U. K.; Jeżowska-Bojczuk, M.; Kyzioł, A. CuI and CuII complexes with phosphine derivatives of fluoroquinolone antibiotics - A comparative study on the cytotoxic mode of action. *J. Inorg. Biochem.* **2018**, *181*, 1−10.
(18) Tyagi, P.; Tyagi, M.; Agrawal, S.; Chandra, S.; Ojha, H.; Pathak, M. Synthesis, characterization of 1,2,4-triazole Schiff base derived 3d-metal complexes: Induces cytotoxicity in HepG2, MCF-7 cell line, BSA binding fluorescence and DFT study. *Spectrochim. Acta, Part A* **2017**, *171*, 246−257.
(19) Zanvettor, N. T.; Nakahata, D. H.; de Paiva, R. E. F.; Ribeiro, M. A.; Cuin, A.; Corbi, P. P.; Formiga, A. L. B. Copper(II), palladium(II) and platinum(II) complexes with 2,2-thiophen-yl-imidazole: Synthesis, spectroscopic characterization, X-ray crystallographic studies and interactions with calf-thymus DNA. *Inorg. Chim. Acta* **2016**, *443*, 304−315.
(20) Viqueira, J.; Durán, M. L.; García-Vázquez, J. A.; Castro, J.; Platas-Iglesias, C.; Esteban-Gómez, D.; Alzuet-Piña, G.; Moldes, A.; Nascimento, O. R. Modulating the DNA cleavage ability of copper(ii) Schiff bases through ternary complex formation. *New J. Chem.* **2018**, *42* (18), 15170−15183.
(21) Silva, P. P.; Guerra, W.; dos Santos, G. C.; Fernandes, N. G.; Silveira, J. N.; da Costa Ferreira, A. M.; Bortolotto, T.; Terenzi, H.; Bortoluzzi, A. J.; Neves, A.; Pereira-Maia, E. C. Correlation between DNA interactions and cytotoxic activity of four new ternary compounds of copper(II) with N-donor heterocyclic ligands. *J. Inorg. Biochem.* **2014**, *132*, 67−76.
(22) Patil, S. A.; Prabhakara, C. T.; Halasangi, B. M.; Toragalmath, S. S.; Badami, P. S. DNA cleavage, antibacterial, antifungal and anthelmintic studies of Co(II), Ni(II) and Cu(II) complexes of coumarin Schiff bases: Synthesis and spectral approach. *Spectrochim. Acta, Part A* **2015**, *137*, 641−651.
(23) Łodyga-Chruscińska, E.; Pilo, M.; Zucca, A.; Garribba, E.; Klewicka, E.; Rowińska-Żyrek, M.; Symonowicz, M.; Chrusciński, L.; Cheshchevik, V. T. Physicochemical, antioxidant, DNA cleaving properties and antimicrobial activity of fisetin-copper chelates. *J. Inorg. Biochem.* **2018**, *180*, 101−118.
(24) Klabunde, T.; Eicken, C.; Sacchettini, J. C.; Krebs, B. Crystal structure of a plant catechol oxidase containing a dicopper center. *Nat. Struct. Biol.* **1998**, *5* (12), 1084−90.
(25) Koval, I. A.; Gamez, P.; Belle, C.; Selmeczi, K.; Reedijk, J. Synthetic models of the active site of catecholoxidase: mechanistic studies. *Chem. Soc. Rev.* **2006**, *35* (9), 814−840.
(26) Rey, N. A.; Neves, A.; Bortoluzzi, A. J.; Haase, W.; Tomkowicz, Z. Doubly phenoxo-hydroxo-bridged dicopper(II) complexes: individual contributions of the bridges to antiferromagnetic coupling based on two related biomimetic models for catechol oxidases. *Dalton Trans.* **2012**, *41* (24), 7196−7200.
(27) Rey, N. A.; Neves, A.; Bortoluzzi, A. J.; Pich, C. T.; Terenzi, H. Catalytic Promiscuity in Biomimetic Systems: Catecholase-like Activity, Phosphatase-like Activity, and Hydrolytic DNA Cleavage Promoted by a New Dicopper(II) Hydroxo-Bridged Complex. *Inorg. Chem.* **2007**, *46* (2), 348−350.
(28) Rey, N. A.; Neves, A.; de Almeida, W. B.; dos Santos, H. F.; Costa, L. A. S. A promiscuous dicopper(II) system promoting the hydrolysis of bis(2,4-dinitrophenyl)phosphate: Gaining mechanistic insight by means of structural and spectroscopic DFT studies. *Int. J. Quantum Chem.* **2009**, *110* (7), 1432−1442.
(29) Esteves, L. F.; Rey, N. A.; Dos Santos, H. F.; Costa, L. A. S. Theoretical Proposal for the Whole Phosphate Diester Hydrolysis

DOI: 10.1021/acs.inorgchem.9b01195
Inorg. Chem. XXXX, XXX, XXX−XXX

Mechanism Promoted by a Catalytic Promiscuous Dinuclear Copper(II) Complex. *Inorg. Chem.* **2016**, *55* (6), 2806−2818.
(30) Rey, N. A.; Neves, A.; Silva, P. P.; Paula, F. C. S.; Silveira, J. N.; Botelho, F. V.; Vieira, L. Q.; Pich, C. T.; Terenzi, H.; Pereira-Maia, E. C. A synthetic dinuclear copper(II) hydrolase and its potential as antitumoral: cytotoxicity, cellular uptake, and DNA cleavage. *J. Inorg. Biochem.* **2009**, *103* (10), 1323−1330.
(31) Sama, F.; Raizada, M.; Ashafaq, M.; Ahamad, M. N.; Mantasha, I.; Iman, K.; Shahid, M.; Rahisuddin; Arif, R.; Shah, N. A.; Saleh, H. A. M. Synthesis, structure and DNA binding properties of a homodinuclear Cu(II) complex: An experimental and theoretical approach. *J. Mol. Struct.* **2019**, *1176*, 283−289.
(32) Iqbal, M.; Ali, S.; Tahir, M. N.; Muhammad, N.; Shah, N. A.; Sohail, M.; Pandarinathan, V. Synthesis, crystal structure and electrochemical and DNA binding studies of oxygen bridged-copper(II) carboxylate. *J. Mol. Struct.* **2015**, *1093*, 135−143.
(33) Jayamani, A.; Sengottuvelan, N.; Kang, S. K.; Kim, Y.-I. Mono- and binuclear copper(II) complexes of the bipyridine ligand: Structural, electrochemical and biological studies. *Polyhedron* **2015**, *98*, 203−216.
(34) Tishchenko, K.; Beloglazkina, E.; Proskurnin, M.; Malinnikov, V.; Guk, D.; Muratova, M.; Krasnovskaya, O.; Udina, A.; Skvortsov, D.; Shafikov, R. R.; Ivanenkov, Y.; Aladinskiy, V.; Sorokin, I.; Gromov, O.; Majouga, A.; Zyk, N. New copper(II) thiohydantoin complexes: Synthesis, characterization, and assessment of their interaction with bovine serum albumin and DNA. *J. Inorg. Biochem.* **2017**, *175*, 190−197.
(35) Zheng, K.; Yan, M. X.; Li, Y. T.; Wu, Z. Y.; Yan, C. W. Synthesis and structure of new dicopper(II) complexes bridged by N-(2-hydroxy-5-methylphenyl)-N'-[3-(dimethylamino)propyl]oxamide with in vitro anticancer activity: A comparative study of reactivities towards DNA/protein by molecular docking and experimental assays. *Eur. J. Med. Chem.* **2016**, *109*, 47−58.
(36) Xu, X. W.; Li, X. J.; Zhu, L.; Li, Y. T.; Wu, Z. Y.; Yan, C. W. Synthesis and structure of dicopper(II) complexes bridged by N-(5-chloro-2-hydroxyphenyl)-N'-[3-(methy lamino)propyl]oxamide: evaluation of DNA/protein binding, DNA cleavage, and in vitro anticancer activity. *J. Photochem. Photobiol., B* **2015**, *147*, 9−23.
(37) Zhao, F.-J.; Zhao, H.-Q.; Liu, F.; Li, Y.-T.; Wu, Z.-Y.; Yan, C.-W. Synthesis and crystal structure of new dicopper(II) complexes with N,N'bis-(dipropylenetriamine)oxamide as bridging ligand: Effects of the counterions on DNA/protein-binding property and in vitro antitumor activity. *J. Photochem. Photobiol., B* **2015**, *143*, 148−162.
(38) Zheng, K.; Zhu, L.; Li, Y.-T.; Wu, Z.-Y.; Yan, C.-W. Synthesis and crystal structure of new dicopper(II) complexes having asymmetric N,N'bis(substituted)oxamides with DNA/protein binding ability: In vitro anticancer activity and molecular docking studies. *J. Photochem. Photobiol., B* **2015**, *149*, 129−142.
(39) Zhu, L.; Zheng, K.; Li, Y. T.; Wu, Z. Y.; Yan, C. W. Synthesis and structure elucidation of new μ-oxamido-bridged dicopper(II) complex with in vitro anticancer activity: A combined study from experiment verification and docking calculation on DNA/protein-binding property. *J. Photochem. Photobiol., B* **2016**, *155*, 86−97.
(40) Sureshbabu, P.; Junaid, Q. M.; Upadhyay, C.; Victoria, W.; Pitchavel, V.; Natarajan, S.; Sabiah, S. Di and tetranuclear Cu(II) complexes with simple 2-aminoethylpyridine: Magnetic properties, phosphodiester hydrolysis, DNA binding/cleavage, cytotoxicity and catecholase activity. *Polyhedron* **2019**, *164*, 202−218.
(41) Ferreira, B. J. M. L.; Brandão, P.; Meireles, M.; Martel, F.; Correia-Branco, A.; Fernandes, D. M.; Santos, T. M.; Félix, V. Synthesis, structural characterization, cytotoxic properties and DNA binding of a dinuclear copper(II) complex. *J. Inorg. Biochem.* **2016**, *161*, 9−17.
(42) Bera, P.; Brandão, P.; Mondal, G.; Santra, A.; Jana, A.; Mokhamatam, R. B.; Manna, S. K.; Mandal, T. K.; Bera, P. An unusual iminoacylation of 2-amino pyridyl thiazole: Synthesis, X-ray crystallography and DFT study of copper(II) amidine complexes and their cytotoxicity, DNA binding and cleavage study. *Polyhedron* **2019**, *159*, 436−445.
(43) Li, M.; Kong, L. L.; Gou, Y.; Yang, F.; Liang, H. DNA binding, cytotoxicity and apoptosis induction activity of a mixed-ligand copper(II) complex with taurine Schiff base and imidazole. *Spectrochim. Acta, Part A* **2014**, *128*, 686−93.
(44) Hernández-Gil, J.; Ferrer, S.; Castiñeiras, A.; Liu-González, M.; Lloret, F.; Ribes, A.; Coga, L.; Bernecker, A.; Mareque-Rivas, J. C. Two novel ternary dicopper(II) μ-guanazole complexes with aromatic amines strongly activated by quantum dots for DNA cleavage. *Inorg. Chem.* **2014**, *53* (1), 578−93.
(45) Montagner, D.; Gandin, V.; Marzano, C.; Erxleben, A. DNA damage and induction of apoptosis in pancreatic cancer cells by a new dinuclear bis(triazacyclonane) copper complex. *J. Inorg. Biochem.* **2015**, *145*, 101−7.
(46) Cao, S.; Cheng, R.; Wang, D.; Zhao, Y.; Tang, R.; Yang, X.; Chen, J. Dinuclear copper(II) complexes of "end-off" bicompartmental ligands: Alteration of the chelating arms on ligands to regulate the reactivity of the complexes towards DNA. *J. Inorg. Biochem.* **2019**, *192*, 126−139.
(47) Godlewska, S.; Jezierska, J.; Baranowska, K.; Augustin, E.; Dołęga, A. Copper(II) complexes with substituted imidazole and chlorido ligands: X-ray, UV-Vis, magnetic and EPR studies and chemotherapeutic potential. *Polyhedron* **2013**, *65*, 288−297.
(48) Beloglazkina, E. K.; Krasnovskaya, O. O.; Guk, D. A.; Tafeenko, V. A.; Moiseeva, A. A.; Zyk, N. V.; Majouga, A. G. Synthesis, Characterization, and Cytotoxicity of Binuclear Copper(II) Complexes with Tetradentate Nitrogen-Containing Ligands bis-5-(2-Pyridylmethylidene)-3,5-dihydro-4H-imidazol-4-ones. *Polyhedron* **2018**, *148*, 129−137.
(49) Pinho, J. O.; Amaral, J. D.; Castro, R. E.; Rodrigues, C. M. P.; Casini, A.; Soveral, G.; Gaspar, M. M. Copper complex nanoformulations featuring highly promising therapeutic potential in murine melanoma models. *Nanomedicine* **2019**, *14* (7), 835−850.
(50) Kumar, P.; Narasimhan, B. Hydrazides/hydrazones as antimicrobial and anticancer agents in the new millennium. *Mini-Rev. Med. Chem.* **2013**, *13* (7), 971−87.
(51) Jovito, R.; Neves, A.; Bortoluzzi, A. J.; Lanznaster, M.; Drago, V.; Haase, W. A new unsymmetrical dinucleating ligand and its first FeIIIZnII complex: Structure and solid state properties of an unexpected tetranuclear complex containing the [FeIII(μ-OH)2FeIII] structural motif. *Inorg. Chem. Commun.* **2005**, *8* (3), 323−327.
(52) Reis, A. C. D. M.; Freitas, M. C. R.; Resende, J. A. L. C.; Diniz, R.; Rey, N. A. Different coordination patterns for two related unsymmetrical compartmental ligands: crystal structures and IR analysis of [Cu(C21H21O2N3)(OH2)(ClO4)]ClO4·2H2O and [Zn2(C22H21O3N2)(C22H20O3N2)]ClO4. *J. Coord. Chem.* **2014**, *67* (18), 3067−3083.
(53) Isaac, J. A.; Mansour, A. T.; David, R.; Kochem, A.; Philouze, C.; Demeshko, S.; Meyer, F.; Réglier, M.; Simaan, A. J.; Caldarelli, S.; Yemloul, M.; Jamet, H.; Thibon-Pourret, A.; Belle, C. Tetranuclear and dinuclear phenoxido bridged copper complexes based on unsymmetrical thiosemicarbazone ligands. *Dalton Trans.* **2018**, *47* (29), 9665−9676.
(54) Neves, A.; de Brito, M. A.; Vencato, I.; Drago, V.; Griesar, K.; Haase, W. FeIIIFeIII and FeIIFeIII Complexes as Synthetic Analogues for the Oxidized and Reduced Forms of Purple Acid Phosphatases. *Inorg. Chem.* **1996**, *35* (8), 2360−2368.
(55) Neves, A.; Verani, C. N.; de Brito, M. A.; Vencato, I.; Mangrich, A.; Oliva, G.; Souza, D. D. H. F.; Batista, A. A. Copper(II) complexes with (2-hydroxybenzyl-2-pyridylmethyl)amine-Hbpa: syntheses, characterization and crystal structures of the ligand and [Cu(II)(Hbpa)-2](ClO4)2·2H2O. *Inorg. Chim. Acta* **1999**, *290* (2), 207−212.
(56) Karsten, P.; Neves, A.; Bortoluzzi, A. J.; Lanznaster, M.; Drago, V. Synthesis, Structure, Properties, and Phosphatase-Like Activity of the First Heterodinuclear FeIIIMnII Complex with the Unsymmetric Ligand H2BPBPMP as a Model for the PAP in Sweet Potato. *Inorg. Chem.* **2002**, *41* (18), 4624−4626.

DOI: 10.1021/acs.inorgchem.9b01195
Inorg. Chem. XXXX, XXX, XXX−XXX

(57) Geary, W. J. The use of conductivity measurements in organic solvents for the characterisation of coordination compounds. *Coord. Chem. Rev.* **1971**, *7* (1), 81−122.
(58) *CrysAlisPro*; Rigaku Corp.: Tokyo, Japan. 2015.
(59) Sheldrick, G. Crystal structure refinement with SHELXL. *Acta Crystallogr., Sect. C: Struct. Chem.* **2015**, *71* (1), 3−8.
(60) Larson, A. C. In *Crystallographic Computing Techniques*; Ahmed, F. R., Hall, S. R., Huber, C. P., Eds.; Munksgaard: Copenhagen, 1976; pp 291−294.
(61) Blessing, R. An empirical correction for absorption anisotropy. *Acta Crystallogr., Sect. A: Found. Crystallogr.* **1995**, *51* (1), 33−38.
(62) Macrae, C. F.; Edgington, P. R.; McCabe, P.; Pidcock, E.; Shields, G. P.; Taylor, R.; Towler, M.; van de Streek, J. Mercury: visualization and analysis of crystal structures. *J. Appl. Crystallogr.* **2006**, *39* (3), 453−457.
(63) Spek, A. L. PLATON SQUEEZE: a tool for the calculation of the disordered solvent contribution to the calculated structure factors. *Acta Crystallogr., Sect. C: Struct. Chem.* **2015**, *71* (1), 9−18.
(64) https://www.sisweb.com/mstools/isotope.htm (accessed April 18, 2019).
(65) Mohanraj, M.; Ayyannan, G.; Raja, G.; Jayabalakrishnan, C. Evaluation of DNA binding, DNA cleavage, protein binding, radical scavenging and in vitro cytotoxic activities of ruthenium(II) complexes containing 2,4-dihydroxy benzylidene ligands. *Mater. Sci. Eng., C* **2016**, *69*, 1297−306.
(66) Ramachandran, E.; Gandin, V.; Bertani, R.; Sgarbossa, P.; Natarajan, K.; Bhuvanesh, N. S. P.; Venzo, A.; Zoleo, A.; Glisenti, A.; Dolmella, A.; Albinati, A.; Marzano, C. Synthesis, characterization and cytotoxic activity of novel copper(II) complexes with aroylhydrazone derivatives of 2-Oxo-1,2-dihydrobenzo[h]quinoline-3-carbaldehyde. *J. Inorg. Biochem.* **2018**, *182*, 18−28.
(67) Hammouda, B. SANS from homogeneous polymer mixtures: A unified overview. *Polymer Characteristics*; Springer: Berlin, 1993; pp 87−133.
(68) Silva, E. R.; Listik, E.; Han, S. W.; Alves, W. A.; Soares, B. M.; Reza, M.; Ruokolainen, J.; Hamley, I. W. Sequence length dependence in arginine/phenylalanine oligopeptides: Implications for self-assembly and cytotoxicity. *Biophys. Chem.* **2018**, *233*, 1−12.
(69) Bressler, I.; Kohlbrecher, J.; Thunemann, A. F. SASfit: a tool for small-angle scattering data analysis using a library of analytical expressions. *J. Appl. Crystallogr.* **2015**, *48* (5), 1587−1598.
(70) Rico, M.; Baglioni, M.; Bondarenko, M.; Laluce, N. C.; Rozados, V.; André, N.; Carré, M.; Scharovsky, O. G.; Márquez, M. M. Metformin and propranolol combination prevents cancer progression and metastasis in different breast cancer models. *Oncotarget* **2017**, *8* (2), 2874−2889.
(71) Landge, S. M.; Tkatchouk, E.; Benítez, D.; Lanfranchi, D. A.; Elhabiri, M.; Goddard, W. A.; Aprahamian, I. Isomerization Mechanism in Hydrazone-Based Rotary Switches: Lateral Shift, Rotation, or Tautomerization? *J. Am. Chem. Soc.* **2011**, *133* (25), 9812−9823.
(72) Kuodis, Z.; Rutavičius, A.; Matijoška, A.; Eicher-Lorka, O. Synthesis and isomerism of hydrazones of 2-(5-thioxo-4,5-dihydro-1,3,4-thiadiazol-2-ylthio)acetohydrazide. *Central Eur. J. Chem.* **2007**, *5* (4), 996−1006.
(73) Palla, G.; Predieri, G.; Domiano, P.; Vignali, C.; Turner, W. Conformational behaviour and E/Z isomerization of N-acyl and N-aroylhydrazones. *Tetrahedron* **1986**, *42* (13), 3649−3654.
(74) Balachandran, V.; Janaki, A.; Nataraj, A. Theoretical investigations on molecular structure, vibrational spectra, HOMO, LUMO, NBO analysis and hyperpolarizability calculations of thiophene-2-carbohydrazide. *Spectrochim. Acta, Part A* **2014**, *118*, 321−330.
(75) Carter, D. C.; Ho, J. X. Structure of Serum Albumin. In *Advances in Protein Chemistry*; Anfinsen, C. B.; Edsall, J. T.; Richards, F. M.; Eisenberg, D. S., Eds.; Academic Press, 1994; Vol. *45*, pp 153−203.
(76) Steinhardt, J.; Krijn, J.; Leidy, J. G. Differences between bovine and human serum albumins. Binding isotherms, optical rotatory dispersion, viscosity, hydrogen ion titration, and fluorescence effects. *Biochemistry* **1971**, *10* (22), 4005−4015.
(77) Kumar, S.; Sharma, R. P.; Venugopalan, P.; Ferretti, V.; Perontsis, S.; Psomas, G. Copper(II) diclofenac complexes: Synthesis, structural studies and interaction with albumins and calf-thymus DNA. *J. Inorg. Biochem.* **2018**, *187*, 97−108.
(78) Kongot, M.; Reddy, D.; Singh, V.; Patel, R.; Singhal, N. K.; Kumar, A. Potent drug candidature of an ONS donor tethered copper (II) complex: Anticancer activity, cytotoxicity and spectroscopically approached BSA binding studies. *Spectrochim. Acta, Part A* **2019**, *212*, 330−342.
(79) Zhang, D.-Y.; Nie, Y.; Sang, H.; Suo, J.-J.; Li, Z.-J.; Gu, W.; Tian, J.-L.; Liu, X.; Yan, S.-P. Three structurally related Copper complexes with two isomers: DNA/BSA binding ability, DNA cleavage activity and excellent cytotoxicity. *Inorg. Chim. Acta* **2017**, *457*, 7−18.
(80) Zarei, L.; Asadi, Z.; Dusek, M.; Eigner, V. Homodinuclear Ni (II) and Cu (II) Schiff base complexes derived from O-vanillin with a pyrazole bridge: Preparation, crystal structures, DNA and protein (BSA) binding, DNA cleavage, molecular docking and cytotoxicity study. *J. Photochem. Photobiol., A* **2019**, *374*, 145−160.
(81) Hazra, M.; Dolai, T.; Pandey, A.; Dey, S. K.; Patra, A. Fluorescent copper(II) complexes: The electron transfer mechanism, interaction with bovine serum albumin (BSA) and antibacterial activity. *J. Saudi Chem. Soc.* **2017**, *21*, S240−S247.
(82) Anjomshoa, M.; Torkzadeh-Mahani, M.; Janczak, J.; Rizzoli, C.; Sahihi, M.; Ataei, F.; Dehkhodaei, M. Synthesis, crystal structure and Hirshfeld surface analysis of copper(II) complexes: DNA- and BSA-binding, molecular modeling, cell imaging and cytotoxicity. *Polyhedron* **2016**, *119*, 23−38.
(83) Anjomshoa, M.; Torkzadeh-Mahani, M. In vitro DNA and BSA-binding, cell imaging and anticancer activity against human carcinoma cell lines of mixed ligand copper(II) complexes. *Spectrochim. Acta, Part A* **2015**, *150*, 390−402.
(84) Annaraj, B.; Balakrishnan, C.; Neelakantan, M. A. Synthesis, structure information, DNA/BSA binding affinity and in vitro cytotoxic studies of mixed ligand copper(II) complexes containing a phenylalanine derivative and diimine co-ligands. *J. Photochem. Photobiol., B* **2016**, *160*, 278−291.
(85) Kostelidou, A.; Kalogiannis, S.; Begou, O.-A.; Perdih, F.; Turel, I.; Psomas, G. Synthesis, structure and biological activity of copper(II) complexes with gatifloxacin. *Polyhedron* **2016**, *119*, 359−370.
(86) Kumar, M.; Masram, D. T. Evaluation of DNA, BSA, and HSA binding propensity of copper(II) complex with N-donor ligand 2,2'dipyridylamine. *Polyhedron* **2019**, *157*, 511−520.
(87) Kumar, M.; Kumar, G.; Mogha, N. K.; Jain, R.; Hussain, F.; Masram, D. T. Structure, DNA/proteins binding, docking and cytotoxicity studies of copper(II) complexes with the first quinolone drug nalidixic acid and 2,2'-dipyridylamine. *Spectrochim. Acta, Part A* **2019**, *212*, 94−104.
(88) Kumar, M.; Mogha, N. K.; Kumar, G.; Hussain, F.; Masram, D. T. Biological evaluation of copper(II) complex with nalidixic acid and 2,2'bipyridine (bpy). *Inorg. Chim. Acta* **2019**, *490*, 144−154.
(89) Manna, S.; Zangrando, E.; Puschmann, H.; Manna, S. C. Tetranuclear Schiff base copper(II) complexes: Syntheses, crystal structure, DNA/protein binding and catecholase-like activity. *Polyhedron* **2019**, *162*, 285−292.
(90) Bhat, S. S.; Kumbhar, A. A.; Heptullah, H.; Khan, A. A.; Gobre, V. V.; Gejji, S. P.; Puranik, V. G. Synthesis, Electronic Structure, DNA and Protein Binding, DNA Cleavage, and Anticancer Activity of Fluorophore-Labeled Copper(II) Complexes. *Inorg. Chem.* **2011**, *50* (2), 545−558.
(91) Jash, C.; Kumar, G. S. Binding of alkaloids berberine, palmatine and coralyne to lysozyme: a combined structural and thermodynamic study. *RSC Adv.* **2014**, *4* (24), 12514−12525.
(92) Yang, Y.; Guo, L.; Tian, Z.; Gong, Y.; Zheng, H.; Zhang, S.; Xu, Z.; Ge, X.; Liu, Z. Novel and Versatile Imine-N-Heterocyclic Carbene Half-Sandwich Iridium(III) Complexes as Lysosome-Targeted Anticancer Agents. *Inorg. Chem.* **2018**, *57* (17), 11087−11098.

DOI: 10.1021/acs.inorgchem.9b01195
Inorg. Chem. XXXX, XXX, XXX−XXX

(93) Pacheco, M. E.; Bruzzone, L. Synchronous fluorescence spectrometry: Conformational investigation or inner filter effect? *J. Lumin.* **2013**, *137*, 138−142.
(94) Ciotta, E.; Prosposito, P.; Pizzoferrato, R. Positive curvature in Stern-Volmer plot described by a generalized model for static quenching. *J. Lumin.* **2019**, *206*, 518−522.
(95) Li, Y.; Guo, Q.; Yan, Y.; Chen, T.; Du, C.; Du, H. Different effects of Forsythia suspensa metabolites on bovine serum albumin (BSA). *Spectrochim. Acta, Part A* **2019**, *214*, 309−319.
(96) Chipman, D. M.; Grisaro, V.; Sharon, N. The binding of oligosaccharides containing N-acetylglucosamine and N-acetylmuramic acid to lysozyme. The specificity of binding subsites. *J. Biol. Chem.* **1967**, *242* (19), 4388−4394.
(97) Dostani, M.; Kianfar, A. H.; Mahmood, W. A.; Dinari, M.; Farrokhpour, H.; Sabzalian, M. R.; Abyar, F.; Azarian, M. H. An experimental and theoretical study on the interaction of DNA and BSA with novel Ni(2+), Cu(2+) and VO(2+) complexes derived from vanillin bidentate Schiff base ligand. *Spectrochim. Acta, Part A* **2017**, *180*, 144−153.
(98) Fu, H.-L.; Zheng, K.; Zhang, M.-J.; Li, Y.-T.; Wu, Z.-Y.; Yan, C.-W. Synthesis and structure of new tetracopper(II) complexes with N-benzoate-N'[3-(diethylamino)propyl]oxamide as a bridging ligand: The influence of hydrophobicity on enhanced DNA/BSA-binding and anticancer activity. *J. Photochem. Photobiol., B* **2016**, *161*, 80−90.
(99) Liu, Y.; Chen, M.; Jiang, L.; Song, L. Stereoselective interaction of cinchona alkaloid isomers with bovine serum albumin. *Food Chem.* **2015**, *181*, 170−178.
(100) Li, Y.; Yang, G.; Mei, Z. Spectroscopic and dynamic light scattering studies of the interaction between pterodontic acid and bovine serum albumin. *Acta Pharm. Sin. B* **2012**, *2* (1), 53−59.
(101) Yu, M.; Ding, Z.; Jiang, F.; Ding, X.; Sun, J.; Chen, S.; Lv, G. Analysis of binding interaction between pegylated puerarin and bovine serum albumin by spectroscopic methods and dynamic light scattering. *Spectrochim. Acta, Part A* **2011**, *83* (1), 453−460.
(102) Cai, H.-H.; Zhong, X.; Yang, P.-H.; Wei, W.; Chen, J.; Cai, J. Probing site-selective binding of rhodamine B to bovine serum albumin. *Colloids Surf., A* **2010**, *372* (1), 35−40.
(103) Adel, A.; Nadia, M.; Mohamed, O.; Abdelhafidh, G. Study of thermally and chemically unfolded conformations of bovine serum albumin by means of dynamic light scattering. *Mater. Sci. Eng., C* **2008**, *28* (5−6), 594−600.
(104) Zocchi, G. Proteins unfold in steps. *Proc. Natl. Acad. Sci. U. S. A.* **1997**, *94* (20), 10647.
(105) Mohanraj, M.; Ayyannan, G.; Raja, G.; Jayabalakrishnan, C. Evaluation of DNA binding, DNA cleavage, protein binding, radical scavenging and in vitro cytotoxic activities of ruthenium(II) complexes containing 2,4-dihydroxy benzylidene ligands. *Mater. Sci. Eng., C* **2016**, *69*, 1297−1306.
(106) Zanvettor, N. T.; Nakahata, D. H.; de Paiva, R. E. F.; Ribeiro, M. A.; Cuin, A.; Corbi, P. P.; Formiga, A. L. B. Copper(II), palladium(II) and platinum(II) complexes with 2,2-thiophen-yl-imidazole: Synthesis, spectroscopic characterization, X-ray crystallographic studies and interactions with calf-thymus DNA. *Inorg. Chim. Acta* **2016**, *443*, 304−315.
(107) García-Zubiri, I. X.; Burrows, H. D.; Sérgio Seixas de Melo, J.; Pina, J.; Monteserín, M.; Tapia, M. J. Effects of the Interaction Between *β*-Carboline-3-carboxylic acid N-Methylamide and Polynucleotides on Singlet Oxygen Quantum Yield and DNA Oxidative Damage. *Photochem. Photobiol.* **2007**, *83* (6), 1455−1464.
(108) Mandal, A.; Bhattacharya, P.; Das, A. K.; Basak, A. A Garratt-Braverman cyclization route towards the synthesis of phenanthridine derivatives and their DNA-binding studies. *Tetrahedron* **2019**, *75* (13), 1975−1987.
(109) Vardevanyan, P. O.; Antonyan, A. P.; Parsadanyan, M. A.; Davtyan, H. G.; Karapetyan, A. T. The binding of ethidium bromide with DNA: interaction with single- and double-stranded structures. *Exp. Mol. Med.* **2003**, *35* (6), 527−33.
(110) Murali Krishna, P.; Hussain Reddy, K.; Pandey, J. P.; Siddavattam, D. Synthesis, characterization, DNA binding and nuclease activity of binuclear copper(II) complexes of cuminaldehyde thiosemicarbazones. *Transition Met. Chem.* **2008**, *33*, 661−668.
(111) Tan, J.; Wang, B.; Zhu, L. DNA binding and oxidative DNA damage induced by a quercetin copper(II) complex: potential mechanism of its antitumor properties. *JBIC, J. Biol. Inorg. Chem.* **2009**, *14* (5), 727−39.
(112) Sundaravadivel, E.; Kandaswamy, M. Synthesis, characterization and electrochemical properties of binuclear copper(II) complexes: DNA/protein binding and DNA cleavage studies. *Mater. Today: Proc.* **2018**, *5*, 8707−8717.
(113) Minton, A. P. Recent applications of light scattering measurement in the biological and biopharmaceutical sciences. *Anal. Biochem.* **2016**, *501*, 4−22.
(114) Latulippe, D. R.; Zydney, A. L. Radius of gyration of plasmid DNA isoforms from static light scattering. *Biotechnol. Bioeng.* **2010**, *107* (1), 134−142.
(115) Dias, R. S.; Innerlohinger, J.; Glatter, O.; Miguel, M. G.; Lindman, B. Coil-Globule Transition of DNA Molecules Induced by Cationic Surfactants: A Dynamic Light Scattering Study. *J. Phys. Chem. B* **2005**, *109* (20), 10458−10463.

DOI: 10.1021/acs.inorgchem.9b01195
Inorg. Chem. XXXX, XXX, XXX−XXX